REPORT DOCUMENTATION PAGE

Form Approved
OMB No. 0704-0188

1. AGENCY USE ONLY (Leave blank)	2. REPORT DATE	3. REPORT TYPE AND DATES COVERED
	16 June 1999	Annual 01 June98- 31 May 1999

4. TITLE AND SUBTITLE Nondestructive Three-dimensional Microtexture/Strain Quantification in Al-Li 2090

5. FUNDING NUMBERS
N00014-97-1-0557
97PR05416-00

6. AUTHOR(S)

7. PERFORMING ORGANIZATION NAME(S) AND ADDRESS(ES)
Georgia Tech Research Corp., Georgia Institute of Technology

8. PERFORMING ORGANIZATION REPORT NUMBER
2

9. SPONSORING / MONITORING AGENCY NAMES(S) AND ADDRESS(ES)
ONR

10. SPONSORING / MONITORING AGENCY REPORT NUMBER

11. SUPPLEMENTARY NOTES

a. DISTRIBUTION / AVAILABILITY STATEMENT
unlimited

12. DISTRIBUTION CODE

13. ABSTRACT *(Maximum 200 words)*
Results of microtexture mapping of Al-Li 2090 T8E41 are reported. Work is concentrating on identifying origin of fatigue crack deflection.

14. SUBJECT TERMS
aluminum, texture, micro-texture, fatigue cracks

15. NUMBER OF PAGES

16. PRICE CODE

17. SECURITY CLASSIFICATION OF REPORT	18. SECURITY CLASSIFICATION OF THIS PAGE	19. SECURITY CLASSIFICATION OF ABSTRACT	20. LIMITATION OF ABSTRACT
unclassified	unclassified	unclassified	unlimited

Standard Form 298 (Rev. 2-89)
Prescribed by ANSI Std 239-18
298-102

and Address(es). Self-explanatory.

Block 10. Sponsoring/Monitoring Agency Report Number. *(If known)*

Block 11. Supplementary Notes. Enter information not included elsewhere such as: Prepared in cooperation with...; Trans. of ...; To be published... When a report is revised, include a statement whether the new report supersedes or supplements the older report.

information, stamp classification on the top and bottom of the page.

Block 20. Limitation of Abstract. This block must be completed to assign a limitation to the abstract. Enter either UL (unlimited) or SAR (same as report). An entry in this block is necessary if the abstract is to be limited. If blank, the abstract is assumed to be unlimited.

Standard Form 298 Back (Rev. 2-89)

FORM A1-2
AUGMENTATION AWARDS FOR SCIENCE & ENGINEERING RESEARCH TRAINING (ASSERT) REPORTING FORM

The Department of Defense (DOD) requires certain information to evaluate the effectiveness of the AASERT program. By accepting this Grant Modification, which bestows the AASERT funds, the Grantee agrees to provide the information requested below to the Government's technical point of contact by each annual anniversary of the ASSERT award date.

1. Grantee identification data: *(R & T and Grant numbers found on Page 1 of Grant)*

   a. GEORGIA TECH RESEARCH CORPORATION GEORGIA INSTITUTE OF TECHNOLOGY
   University Name

   b. N00014-97-1-0557 — Grant Number
   c. 97PR05416-00 — PR Number

   d. Stuart R. Stock — P.I. Name
   e. From: 01 JUN 97 To: 31 MAY 00 — AASERT Reporting Period

NOTE: Grant to which AASERT award is attached is referred to hereafter as "Parent Agreement."

2. Total funding of the Parent Agreement and the number of full-time equivalent graduate students (FTEGS) supported by the Parent Agreement during the 12-month period **prior to** the AASERT award date.

   a. Funding: $71,400

   b. Number FTEGS: 1

3. Total funding of the Parent Agreement and the number of FTEGS supported by the Parent Agreement during the current 12-month reporting period.

   a. Funding: $ 72,000

   b. Number FTEGS: 0

4. Total AASERT funding and the number of FTEGS and undergraduate students (UGS) supported by AASERT funds during the current 12-month reporting period.

   a. Funding: $ 35,000

   b. Number FTEGS: 0.5

   c. Number UGS: 2

VERIFICATION STATEMENT: I hereby verify that all students supported by the AASERT award are U.S. citizens.

Stuart R. Stock
Principal Investigator

6/16/99
Date

GRANT NUMBER: N00014-97-1-0557

Annual Report for AASERT Program N00014-97-1-0557, "Nondestructive Three-Dimensional Microtexture/Strain Quantification in Al-Li 2090."

Stuart R. Stock
Associate Professor
School of Materials Science and Engineering
Georgia Institute of Technology
Atlanta, Georgia 30332-0245

One US citizen's graduate work was supported during the past year: Mr. R. Morano. His MS was completed in September 1998 (R. Morano, 1998, "Effect of R-ratio on Crack Closure in Al-Li 2090 T8E41, Investigated Non- destructively with X-ray Micro-Tomography."), and he is currently ENS-Candidate USN. A second MS thesis, based on work of Mr. C.P. Patterson II who was supported by the predecessor AASERT grant, should be defended Summer 1999. Two US citizens have been employed as undergraduate research assistants: Ms. Chekesha Bradford and Mr. Tony Watt. Both graduated June 1999. Ms. Bradford won a NSF Graduate Fellowship, which she declined, and a DOD Graduate Fellowship, which she accepted. Note she is an African-American student. Finally the project director, Dr. S.R. Stock, was promoted to Professor from Associate Professor, effective August 1999.

Research employed synchrotron polychromatic microbeams to map microtexture in three-dimensions in Al-Li 2090. The results expanded on earlier observations and are communicated in the publications tabulated below. Also of considerable interest was the demonstration that the synchrotron microbeams could produce transmission Laue patterns in reasonable times through 2-3 mm thicknesses of Ti-6Al-4V; this means that the techniques developed in this program will have much greater use in materials of interest to ONR. Two invited presentations were given and a conference proceeding was edited by the project director appeared (Applications of Synchrotron Radiation Techniques to Materials Science IV, Materials Research Society Symposium Proceedings Volume 524, 1998, Susan M. Mini, Stuart R. Stock, Dale L. Perry and Louis J. Terminello, Eds., 383 pages). Five papers were published, and five are in press. Copies of the papers in print form the body of this report.

Publications listed previously "in press": Title, authors, bibliographic data

1. "X-ray Microbeam Mapping of Microtexture Related to Fatigue Crack Asperities in Al-Li 2090," J.D. Haase, A. Guvenilir, J.R.Witt and S.R. Stock, Acta Mater, **46** (1998) 4791-4799.
2. "Micro-, Meso- and Macro-texture and Fatigue Crack Roughness in Al-Li 2090 T8E41," J.D. Haase, A. Guvenilir, J.R. Witt and S. R. Stock, MRS Symp Proc **524** (1998) 37-42.
3. "X-ray Microbeam Quantification of Grain Subdivision Accompanying Large Deformations of Copper," G.C. Butler, A. Guvenilir, D.L. McDowell and S.R. Stock, MRS Symp Proc **524** (1998) 43-48.

Publications listed previously as submitted: Title, authors, bibliographic data

4. "Microtexture, Asperities and Crack Deflection in Al-Li 2090 T8E41," Jake D. Haase, Abbas Guvenilir, Jason R. Witt, Morten A. Langøy and Stuart R. Stock, in Mixed-Mode Crack Behavior, ASTM STP 1359 (1999) 160-173.
5. "X-ray Microbeam Quantification of Grain Subdivision Accompanying Large Deformations of Copper," A. Guvenilir, G.C. Butler, J.D. Haase, D.L. McDowell and S.R. Stock, Acta Mater **46** (1998) 6599-6604.

Publications submitted and in press: Title, authors, bibliographic data

6. "X-ray Microtomography of Materials," S.R. Stock, International Materials Reviews, in press 1999.
7. "New Direct Observations of Crack Closure Processes in Al-Li 2090 T8E41," A. Guvenilir, T.M. Breunig, J.H. Kinney and S.R. Stock, Phil Trans Royal Society Lon., in press 1999.
8. "Mesotexture, deflection and closure of fatigue cracks in Al-Li 2090 T8E41," S.R. Stock, in Advanced Materials for the 21st Century: The 1999 Julia R. Weertman Symposium, in press 1999.
9. "Macrotexture-related Fatigue Crack Closure in Al-Li 2090 Studied by X-ray Microtomography," R. Morano, S.R. Stock, G.R. Davis and J.C. Elliott, in Proceedings of ICOTOM-12 (12th International Conference on Texture of Materials), in press 1999.
10. "Polychromatic Microbeam Diffraction, Mesotexture and Crack Deflection in Al-Li 2090 T8E41," J.D. Haase, R. Morano, T. Watt and S.R. Stock, in Proceedings of ICOTOM-12 (12th International Conference on Texture of Materials), in press 1999.

Invited presentations:

1. "Three-dimensional Microbeam Diffraction Tomography of Fatigue Crack Asperities in Al-Li 2090," S.R. Stock, ASM International Symposium on Heat Treating, Chicago, IL, October 13, 1998.
2. "X-ray Microtomography and X-ray Microdiffraction," Dept. of Materials Science and Engineering, Ohio State University, May 26, 1999.

Pergamon

Acta mater. Vol. 46, No. 13, pp. 4791–4799, 1998

Printed in Great Britain
PII: S1359-6454(98)00118-9
1359-6454/98 $19.00 + 0.00

X-RAY MICROBEAM MAPPING OF MICROTEXTURE RELATED TO FATIGUE CRACK ASPERITIES IN Al–Li 2090

J. D. HAASE, A. GUVENILIR†, J. R. WITT and S. R. STOCK‡

School of Materials Science and Engineering and Mechanical Properties Research Laboratory, Georgia Institute of Technology, Atlanta, GA 30332-0245, U.S.A.

(Received 6 November 1997; accepted 16 March 1998)

Abstract—In certain orientations, Al–Li 2090 T8E41 cracks more slowly in fatigue than other aluminum alloys due to roughness-induced closure linked to the average texture or macrotexture. For this application, three-dimensional, non-destructive measurement of microtexture and strain evolution within samples was developed using synchrotron polychromatic X-ray microbeam diffraction; its use in mapping the microtexture of fatigue crack asperities in Al–Li 2090 are reported. Groups of adjacent grains with nearly identical orientations were found at numerous locations in the plate centers, and this type of "mesotexture" appeared closely tied to asperity formation. Changing arrangements of 111 diffraction spots relative to the samples' rolling and crack propagation directions are found to correspond to the transitions between a relatively planar section of the crack and an adjacent asperity. © *1998 Acta Metallurgica Inc. Published by Elsevier Science Ltd. All rights reserved.*

1. INTRODUCTION

Knowledge of the three-dimensional distribution of stress, strain, microtexture, etc. is sometimes necessary in order to understand the complex macroscopic behavior of today's engineering materials. More specifically, understanding the role of microtexture and the evolution of strain in response to monotonic and cyclic loading would lead to improved models for predicting a material's macroscopic behavior. One such method under development, three-dimensional microbeam X-ray diffraction tomography [1–4], is being used to investigate Al–Li 2090, an engineering alloy with interesting properties. In this alloy, fatigue crack growth rates along certain plate orientations are unusually low compared to those of other Al alloys [5, 6]. This is related to a characteristic macrotexture (i.e. the texture averaged over a large number of grains) in the center of the plates which produces a rough, asperity dominated crack face and significant crack deflection [7]. The prominent macrotexture of the center of plates of this Al alloy has been correlated with the geometry of asperities on fatigue crack faces [8], but the role of microtexture on the path of fatigue cracks through the solid appears to have received little attention.

Orientation Imaging Microscopy (OIM) is an alternative to the microtexture mapping method used in this work, and it determines crystal orientation from the distribution of backscattered electrons in a scanning electron microscope or SEM [9, 10]. The relatively shallow interaction volume of electrons prevents this method from examining the interior of bulk samples without destructive sample preparation. Another drawback of the OIM method is that it requires special sample preparation; for example, polishing damage must be removed. In contrast, the X-ray microbeams described below allow the sample's entire volume to be mapped nondestructively, an important advantage if the evolving strain accumulation ahead of the crack is also of interest.

The goal of the work reported here is to understand how local changes in the microtexture lead to the low fatigue crack growth rate in Al–Li 2090. To this end, transmission Laue patterns using synchrotron X-ray microbeams were recorded at numerous positions on a compact tension sample. The commissioning of the new high brightness sources ESRF (European Synchrotron Radiation Facility) and APS (Advanced Photon Source) have stimulated others to employ similar approaches to mapping microtexture (e.g. Refs [11, 12]). Emphasis in this paper is on identifying what features or changes in features within the diffraction patterns correlate with asperity formation. In other words, the approach is to determine the location and orientation of individual grains or groups of similarly aligned grains related to asperity formation in Al–Li 2090. Comparison of the observed microtexture associated with a particular large asperity and the macrotexture of Al–Li 2090 demonstrates the present results are consistent with earlier reports.

†Present address: Motorola, M/D K-10 Yield Enhancement Technology Transfer, 3501 Ed Bluestein Blvd, Austin, TX 78721, U.S.A.

‡To whom all correspondence should be addressed.

2. BACKGROUND

One result of the crack face roughness in Al–Li 2090 is crack closure, the phenomenon where the crack faces come into contact prematurely during unloading of the sample (i.e. before the minimum stress of a fatigue cycle is reached) or where the crack faces remain in contact much longer than expected during loading [13]. Crack closure, in combination with significant crack deflection which increases the total crack length, leads to a reduced driving "force" for crack propagation and lower fatigue crack growth rates [14].

In 12.7 mm thick plates of Al–Li 2090 T8E41, the macrotexture of the center of the plate is very different from that in the outer sections [7], and the surfaces of fatigue cracks are much rougher, with larger, steeper asperities in the center than on the outside of the plate. The center region texture is characterized by two strong preferred orientations {123}⟨634⟩ and {110}⟨112⟩ and one weak preferred orientation {112}⟨111⟩; and Yoder *et al.* [8] have shown that the orientations of the faces of the asperities are related to this macrotexture. Using the macrotextural information contained in pole figures, it was determined that the angle between the two faces of large asperities corresponds to that between high density {111} orientations in the pole figure. Thus, the shape of asperities is a direct consequence of the macrotexture.

Given that the morphology of the crack surface relates to the macrotexture present, the question remains: whether asperities in the center of plates of Al–Li 2090 form at random within the volume of material through which the crack is constrained to grow (by the notch) or whether variation in microtexture within this volume dictates where large and small asperities develop. In other words, does the crack choose its path to avoid grains or groups of grains with certain orientations or to grow through individual grains, groups of grains or specific orientations of grain boundaries. The resulting large crack deflections and accompanying fatigue crack closure, which has been measured macroscopically [5, 6] and with high resolution X-ray computed tomography [15–17], are responsible for the very low fatigue crack growth rates in the L–T orientation. Side grooves can minimize crack deflection [Fig. 1(a)], but very large deflections are the rule otherwise [Fig. 1(b)].

3. EXPERIMENTS

Compact tension samples were examined in this study of microtexture: identification of the microtexture producing crack deflection and asperity formation in Al–Li 2090 requires examination of samples with geometries that can be compared with those of other investigators. The compact tension samples had a thickness of 2.7 mm and were

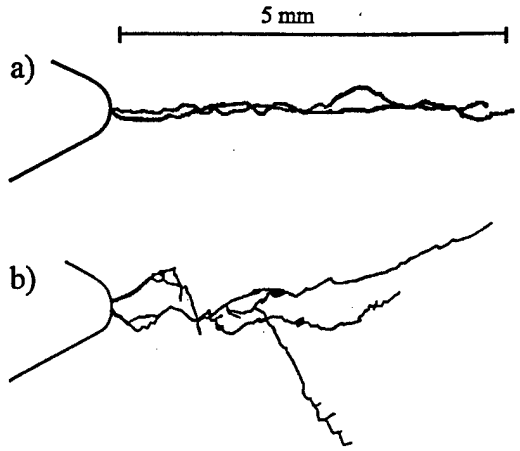

Fig. 1. Crack profiles on the faces of Al–Li 2090 compact tension samples: that on one face is shown in black and on the other in gray. The crack profile at both faces of the grooved sample (CT-2) is shown in (a) while (b) shows the crack path on the front and back surface of a sample without side grooves (CT31). The notch tip is on the left.

machined from the center of plates of Al–Li 2090 T8E41; the specific dimensions are discussed elsewhere [17, 18], but the scaling was in accordance with ASTM E-399-83 [19]. Composition, mechanical properties and fatigue crack growth rates for this material are reported elsewhere [6, 20]. Fatigue cracks were grown in L–T oriented compact tension samples (i.e. loading along the L direction and crack propagation along the T direction) with $R = 0.1$ (i.e. $\sigma_{min}/\sigma_{max}$), 5 Hz frequency and haversine wave form. Most of the samples tested to date had side grooves which minimized crack deflection and allowed valid comparisons to be made with the observations of others of stress intensity range, etc. A number of samples were examined before crack propagation, several were examined after fatigue cracks had extended 6–7 mm and a few specimens were studied after fracture. This paper focuses on the samples which were fractured.

In the fractured samples, the volume of material adjacent to the crack was cut from the sample so that the specimen could be examined in the transmission parallel to the rolling direction (L) (Fig. 2). The sample thicknesses (along L) were kept equal to or less than 3 mm so that the number of overlapping diffraction streaks would not overly complicate analysis nor would exposure times be lengthened inordinately.

The microtexture was mapped in the various compact tension specimens by translating the sample along the two orthogonal axes perpendicular to the beam by fixed increments and recording the resulting transmission Laue pattern. Prior to microbeam data collection, the surfaces of the fractured compact tension samples were viewed optically to locate asperities so that microtexture data collection could concentrate on areas of interest. For the fractured compact tension specimens, most

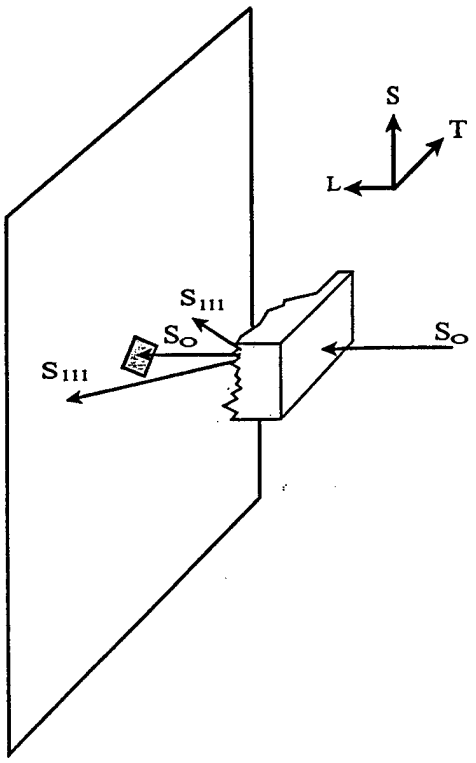

Fig. 2. Experimental geometry with incident X-ray beam parallel to the rolling direction (L). The transverse plate direction T is horizontal. The sample is a section from a fractured compact tension of Al–Li 2090. Incident and exit beams are shown, and the diffracted beams exit the fracture surface.

of the Laue patterns were recorded with the incident beam parallel to the rolling direction (L). In this "parallel" geometry (Fig. 2), the beam was translated along the short transverse (S) direction for various positions along the transverse (T) axis. The fractured compact tension specimens were also examined with the incident beam parallel to the short direction (i.e. perpendicular to the face of the plate and in the "perpendicular" geometry) in order to investigate whether asperities could be located in unfractured, unsectioned compact tension specimens. In samples where both fracture surfaces are available, matching locations on each face were studied with the X-ray microbeams.

All diffraction data were collected with polychromatic bending magnet radiation at Stanford Synchrotron Radiation Laboratory (SSRL) beamline 2–2 (3.0 GeV, beam currents between 20 and 100 mA). Pinhole collimators with 100, 30 or 10 μm diameters have been used. Exposure levels were of the order of 2×10^3 and 1×10^4 mA s for the 100 and 30 mm collimators, respectively. The collimator was placed 55 cm from the sample in order to minimize the effect of scatter from the edges of the pinhole. The ~20 arcseconds of vertical divergence of the beam was enough to broaden the beam from the 10 μm diameter collimator to 80 μm vertically at the sample position. Image storage plates [21,22] were used to record the polycrystalline Laue patterns. Initially, 20×25 cm^2 plates were read with 100 μm pixel size and 1024 levels of contrast in a Fuji BAS-2000 Imaging Plate Scanner. Once a Fuji BAS-2500 Imaging Plate Scanner became available, all data was collected on this system on plates with an area of 20×40 cm^2 and read with 50 μm pixel resolution and 256 levels of contrast. Additional levels of contrast could be obtained in the BAS-2500 system at the cost of much larger data file sizes, but 256 levels of contrast provided adequate range for these experiments.

In Laue patterns of *polycrystalline* samples, each grain produces its own set of spots or streaks, and one cannot easily separate the superimposed patterns. Occasionally there are features in the pattern peculiar to the spots/streaks from a given grain which allow for grain identification, but this approach is not often possible. Instead, the primary goal of indexing the polycrystalline Laue patterns becomes identifying the diffraction planes *hkl* producing the features recorded on the detector or film. Measuring the separation (in the transmission Laue pattern) between the feature of interest and the position where the incident beam exposed the image plate and knowing the distance between sample and detector allows the diffraction angle 2θ to be calculated. Bragg's law (for cubic materials)

$$\lambda = 2d_{hkl} \sin\theta = 2a \sin\theta/(h^2 + k^2 + l^2)^{1/2}$$

where λ is the wavelength, d_{hkl} the interplanar spacing for reflection *hkl* and a is a lattice parameter, can only be used to determine *hkl* if λ is known. In order to identify the positions where one wavelength was diffracted, a filter with an absorption edge in the wavelength range of interest was placed in the beam in some of the patterns. Wavelengths of the polychromatic beam below the filter's absorption edge are heavily attenuated, and these wavelengths no longer contribute appreciably to the Laue pattern. Wavelengths above the edge suffer relatively little attenuation compared to those below the edge. A sharp change in contrast results in the polycrystalline diffraction pattern [23], and this allows the pattern to be indexed (see Fig. 3).

4. RESULTS AND DISCUSSION

In the fractured compact tension specimens, the thickness was chosen so that the number of grains in the beam path along the rolling direction (i.e. in the parallel diffraction geometry) would be minimized. The appearance of complex streaks is evident in microtexture mapping in the parallel geometry and greatly complicated the process of determining the orientation of specific diffracting regions. Since the grain size in Al–Li 2090 along the L direction is of the order of 1 mm and along

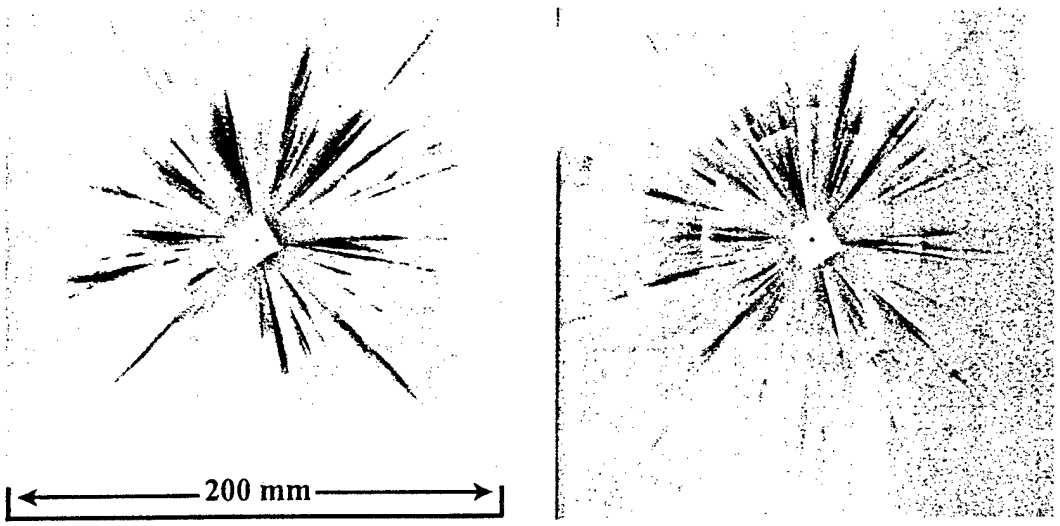

Fig. 3. Two diffraction patterns at the same location on compact tension sample CT21. These patterns were recorded in the perpendicular geometry (i.e. along the short plate direction), the transverse plate direction T is horizontal. A 10 μm diameter collimator was used to form the microbeam. and the pattern on the right was made by placing a 75 μm thick molybdenum filter in the incident beam path. The presence of this filter causes a sharp change in contrast for diffraction of wavelengths above and below 0.62 Å, i.e. at the wavelength of the Mo K-edge. The darker the pixel value in this figure, the greater the diffracted intensity. The white diamond in the center of the pattern is the beam stop and, by design, the incident beam penetrates it. The separation between the exit surface of the sample and the detector was approximately 245 mm.

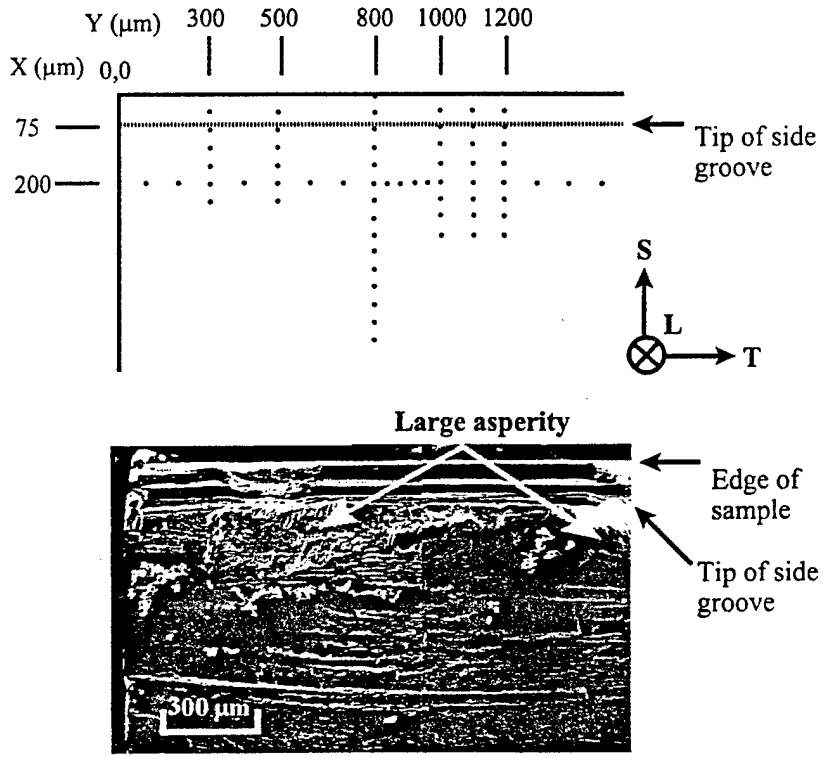

Fig. 4. Map of microbeam position (top) at the same scale as the SEM fractograph (bottom) of compact tension sample CT21 containing the large asperity described in the text and in Figs 5–8. The viewing perpective is normal to the surface, the crack propagated from left to right and one of the side grooves appears at the top of the micrograph.

the S direction is of the order of 50 μm, diffraction patterns from the samples would be expected to consist of streaks from several grains, but not several tens of grains. The separation between sampling positions was chosen so that streaks from each grain would be present in more than one diffraction pattern (i.e. to reveal gradual changes in microtexture) and ranged from 20 to 100 μm. Grouping of 111 streaks is observed in both the parallel and perpendicular geometries, and this suggests that results obtained in the two experimental geometries can be correlated. This is important since the parallel geometry allows straightforward diffraction pattern interpretation and beam position correlation with asperity locations determined by scanning electron or optical microscopy.

Figure 4 juxtaposes a map of microbeam positions and an SEM micrograph of the fracture surface viewed along the loading axis (i.e. normal to the nominal fracture plane). One side groove is visible at the top of the micrograph, and the crack propagated from left to right. The very large asperity described below lies adjacent to the side groove and extends almost the entire length of the micrograph. Identifying specific streaks or clusters of streaks associated with asperities in the perpendicular geometry is much more difficult without the guidance of the results of mapping in the parallel geometry.

Figure 5 shows the same area of the sample as Fig. 4, but the sample is viewed at a large angle of tilt. The white dashed line indicates the position of a scan of the beam along the sample's S direction. Note the large asperity at the top of the SEM micrograph. The center portions of two diffraction patterns are shown to the right of the fractograph, and the arrows indicate the position where each was recorded. In Fig. 3 and Figs 5–9, the diamond at the center of each Laue pattern is a lead beam stop whose thickness was chosen to attenuate most (but not all) of the incident beam; and increasing diffracted intensities are indicated by the darkening of the pattern. The abrupt change of texture at the edge of the asperity is seen by the quite pronounced change in 111 streak orientations to the right of the beam stop. The upper pattern shows streaks oriented from 3 o'clock to 4 o'clock, with the longest and most intense streak being at 4 o'clock, while the lower pattern shows most of the 111 streaks between 2 o'clock and 3 o'clock orientations. Within the volume of asperity, the orientation of the 111 streaks varied little from the upper pattern of Fig. 5. Outside the asperities, the 111 streaks either had different orientations or were not present.

A series of diffraction patterns in the parallel geometry and spanning the asperity along the S direction of the sample is shown in Fig. 6. Only the central portion of the patterns are shown, patterns (a) and (e) are outside the asperity and the difference in diffraction patterns taken from the asperity volume are easily seen compared to those of nearby planar regions of the crack face. This type of mapping allows the entire asperity along both the S and T directions to be covered. Figure 7 shows a series of diffraction patterns taken in the same geometry but with the translation between exposures being along the sample's T direction (i.e. along the length

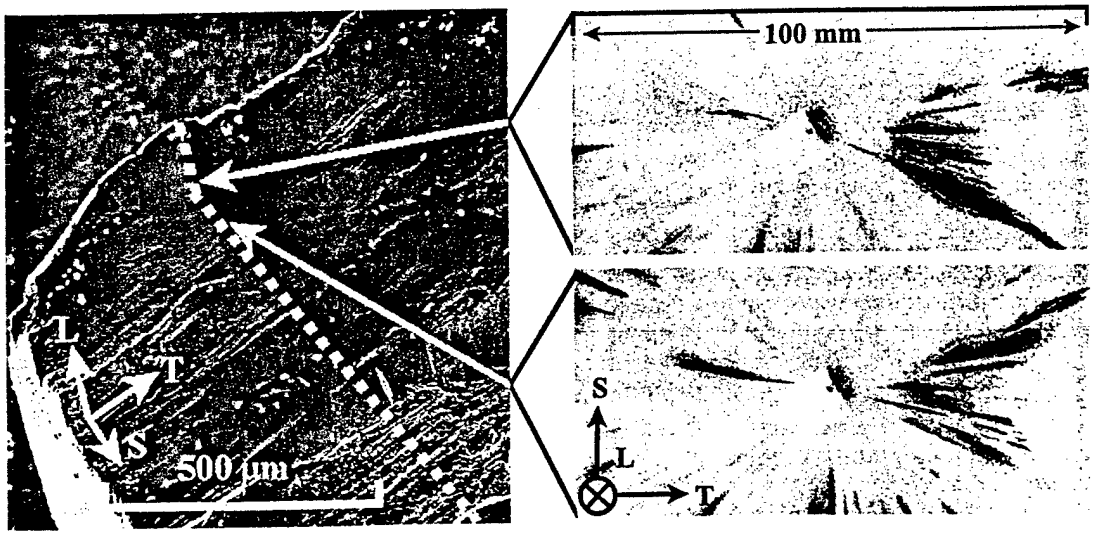

Fig. 5. SEM fractograph of the region of the compact tension sample shown in Fig. 4 but at a high angle of tilt. The large asperity appears at the top, and the dashed line marks the line along which the microbeam was scanned. The central portion of diffraction patterns just within (top right) and just outside (bottom right) the asperity are shown to the right of the fractograph; the two positions are identified by the arrows. The darker the pixel value in these diffraction patterns, the greater the diffracted intensity. The white diamond in the center of the pattern is the beam stop. These diffraction patterns were recorded with a separation of about 245 mm between the exit surface and the detector.

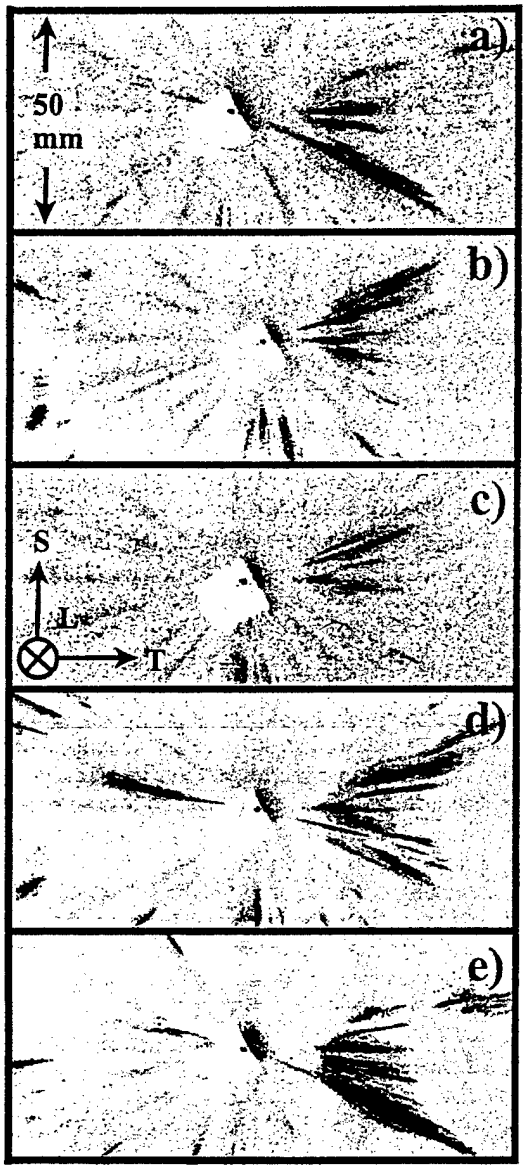

Fig. 6. A series of five diffraction patterns showing the characteristic change in microtexture in and around an asperity in CT21. The images were taken in 50 μm translation steps with a 10 μm diameter collimator beam and translation along the short rolling direction (S) across the asperity. The sample was oriented so that the incident X-ray beam is parallel to the rolling direction. Patterns (b)–(d) are from the asperity region, and the gray scale and sample–detector separation are the same as in Fig. 5.

of the asperity). The microtexture revealed by the 111 streaks changes little over the 250 μm of translation.

Figure 8 shows a series of diffraction patterns of the same asperity shown in Fig. 7 but recorded in the perpendicular geometry (i.e. with the incident X-ray beam parallel to the S direction and normal to the face of the plate). The positions of diffraction patterns in Fig. 8 are separated by 20 μm translations along the sample's T direction. This demonstrates that the microtexture producing the 111 streaks parallel to or nearly parallel to the plate's T direction in the parallel diffraction orientation also can be unambiguously seen in the perpendicular geometry as horizontal 111 streaks. It is likely, therefore, that volumes of material with the proper microtexture to form asperities can be located nondestructively in samples prior to crack growth. Whether or not such volumes of material actually form asperities or significant crack deflection, however, depends on many other factors, including whether the advancing crack will intersect the volume.

It is also important to ascertain whether the microtexture inside and outside of the asperity

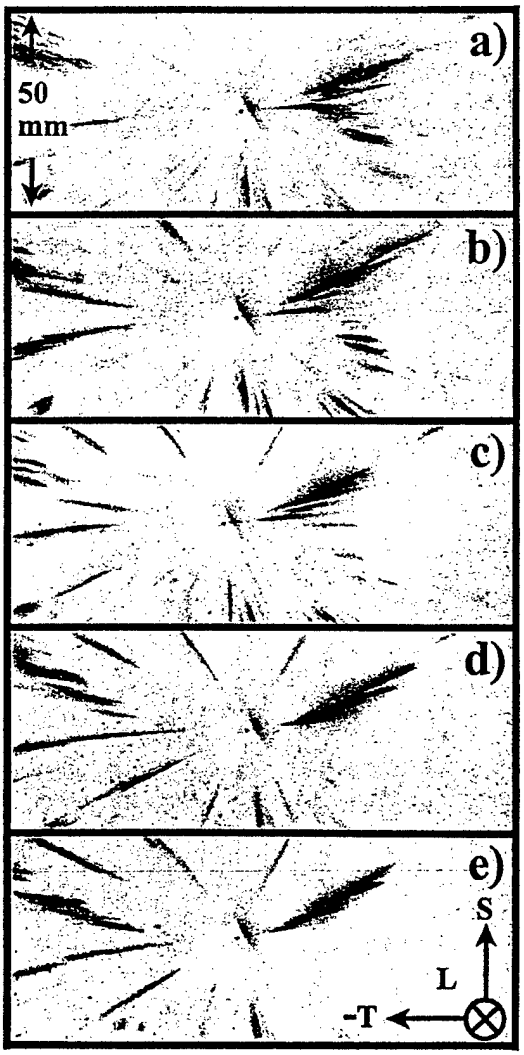

Fig. 7. A series of five diffraction patterns recorded with the 10 μm diameter collimator and showing the ⟨111⟩ streaks comprising the characteristic change in microtexture from an asperity region. The images are from positions within the asperity separated 50 μm apart along the transverse rolling direction (T), and the gray scale and sample–detector separation are the same as in Fig. 5.

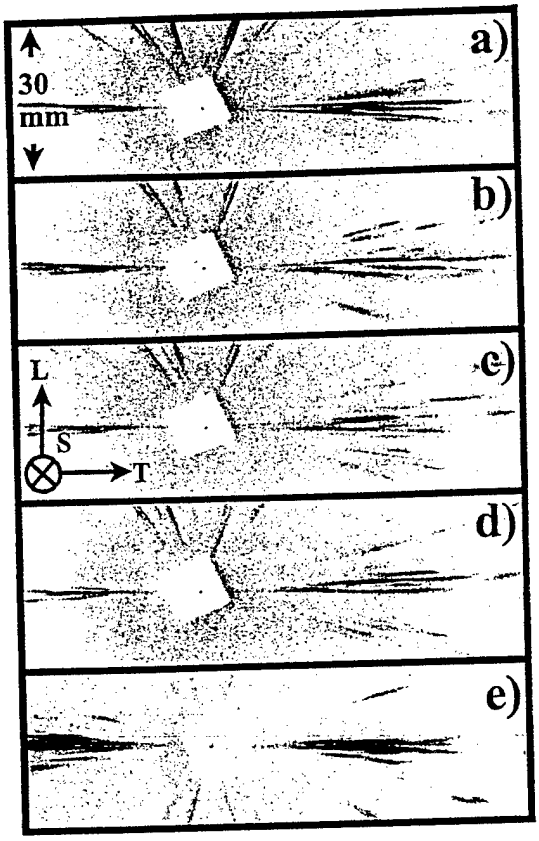

Fig. 8. Portions of perpendicular geometry diffraction patterns recorded at five different positions along the length of an asperity. This asperity was also shown in Figs 6 and 7. Translation was in 20 μm steps along the plate's T direction and the 111 streaks lie along this direction. A 10 μm diameter collimator was used to form the microbeam.

described above is consistent with the expected average texture. Figure 9 shows an experimental 111 pole figure (after Ref. [7]) from the central portion of plates of Al–Li 2090 T8E41. The section of the diffraction patterns just inside and just outside the asperity (Fig. 5) are reproduced, and the arrows link the diffraction patterns with the orientation in the pole figure producing the characteristic streaks. Seeing that these orientations produce exit beams in the proper directions and with the proper diffraction angles requires locating the entrance and diffracted beams (S_0 and S_{111}, respectively) coplanar with and at an angle $\pi/2 - \theta_B$ from the plane normal. Consider the solid rectangle in the right portion of the pole figure as an idealized representation of orientations comprising this portion of the macrotexture, and note that the top and bottom of this region represent those orientations which will produce diffraction streaks at the greatest angle with respect to the transverse direction. Since S_0 is along L for the diffraction patterns shown to the right of the pole figure, constructing a stereographic projection with the reference direction along L (shown below the pole figure) allows straightforward comparison. The rectangle in the pole figure rotates to the position shown, and exit beams S_{111} corresponding to the innermost corners of the solid rectangles are indicated by the dashed lines leading to the outermost corners of the open triangles (on the back of the projection). From this representation of the texture, 111 streaks are expected to be at an angle no greater than $\pm 25°$ from T; experimentally the angles are $\sim +20°$ in the upper pattern and $\sim -25°$ in the lower pattern. Note that there will be a spread of Bragg angles observed, and $90 - \theta_B$ will be 80° for the innermost corner of the rectangle in the stereographic projection. This Bragg angle (10°) corresponds to diffraction of a wavelength of 0.812 Å, and the rest of the grains with 111 orientations represented by the rectangle are expected to diffract at shorter wavelengths. When the molybdenum filter is inserted into the beam, the position of its K-edge (0.62 Å) intersects the 111 streaks near the transverse direction in some of the diffraction patterns, and this confirms the identification of the portion of the macrotexture related to the microtexture inside and outside of the asperity.

A consistent picture emerges of the relationship between microtextrue, macrotexture, asperity formation and "choice" of crack path of the central portion of plates of Al–Li 2090 T8E41. Groups of adjacent, highly-oriented, plate-like grains form near-single-crystal regions within the plate, and this spatial distribution of microtexture is a specific type of mesotexture which defines favored crack paths. In other words, macrotexture describes large-scale average texture (e.g. an average over the sample), microtexture is used to describe the orientations present at the subgrain scale or in a grain-by-grain average and mesotexture is used to describe the average preferred orientation over an assembly of adjacent grains. The present observations are consistent with the distribution of misorientation angles measured across grain boundaries for this material [24]. Numerous studies have demonstrated that deformation is highly planar in Al–Li alloys and that such deformation morphology leads to considerable crystallographic faceting of fracture surfaces. Yoder and co-workers [7, 8] linked the formation of large asperities, through the macrotexture revealed in pole figures, to the crystallography of slip and fracture surfaces. These observations, coupled with the data reported above produce the following view of crack path selection in Al–Li 2090 T8E41: fatigue cracks tend to propagate crystallographically within or adjacent to highly-oriented near-single-crystal volumes and that crack deflection is likely at the boundary of such a region. The relatively high probability that adjacent pancake-shaped grains are nearly aligned leads one to expect fracture features with aspect ratios and orientations similar to that of the individual grains. The correlation between macrotexture and the

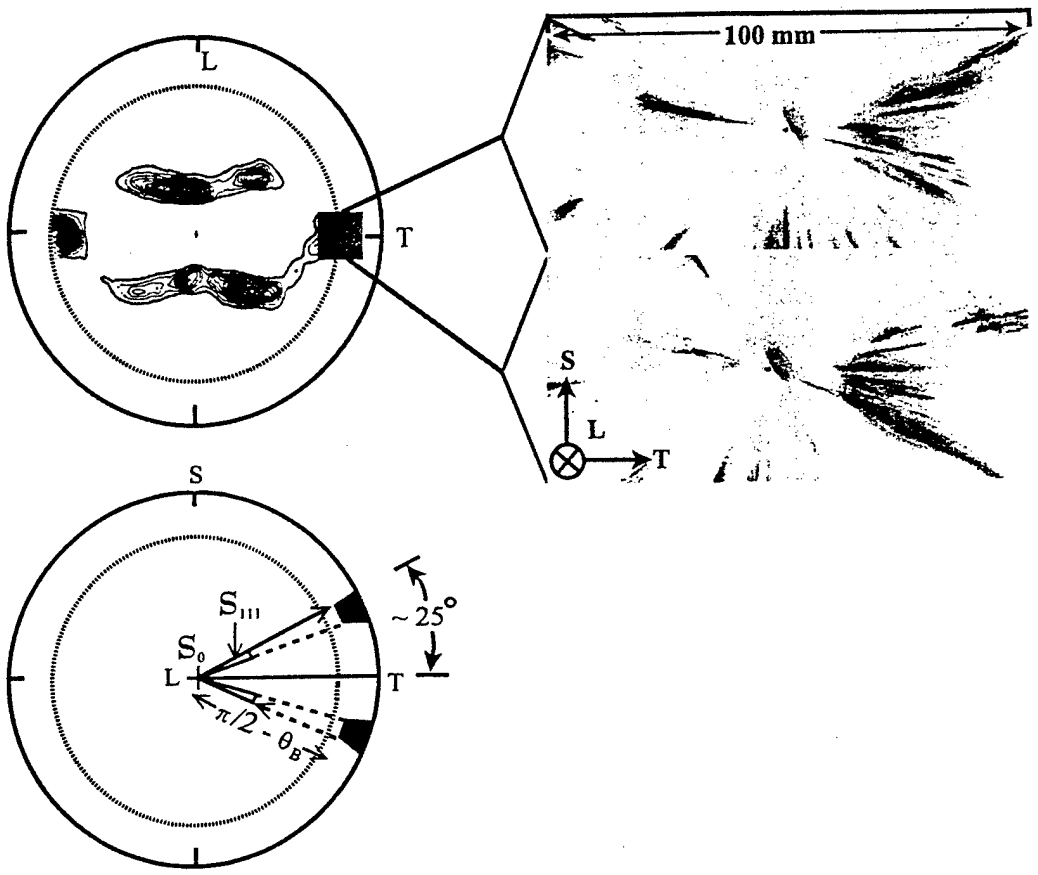

Fig. 9. Orientation of 111 diffraction streaks related to the macrotexture of the center of plates of Al–Li 2090 T8E41. The 111 pole figure (after Ref. [7]) is shown in the upper left, and the portion of the macrotexture producing the 111 streaks associated with the asperity is represented schematically by the solid rectangle on the right-hand side of the pole figure. The centers of two diffraction patterns show the 111 streaks just outside (top right) and inside the asperity (lower right). The L-oriented stereographic projection (lower left) is used to relate the experimentally observed 111 streaks to the macrotexture: the locus of expected diffracted beam directions (i.e. the streaks) from the orientations within the solid rectangle are indicated by the elongated triangles nearly parallel with the T axis.

{111} faces of asperities is, therefore, not surprising. Near-single-crystal regions consisting of multiple grains will tend to act like single crystals, slip across grain boundaries within this region will be relatively easy and the resulting fracture surface will be crystallographic with {111} faces. Thus, the spatial distribution of these highly-oriented regions appears to govern whether or not asperities are present on fatigue crack surfaces in this alloy/heat treatment and where on the surfaces these asperities form.

The observation of mesotexture is consistent with the very low fatigue crack growth rates seen in Al–Li 2090 samples tested in the L–T orientation. Crystallographic crack propagation tends to be considerably slower that transgranular cracking [25]. Further, forcing the fatigue crack out of the nominal plane of the notch would also be expected to slow propagation rates since the area of the fatigue crack would be greatly increased, while the effective crack length would be unchanged. These factors, when coupled with decreased driving "force" from roughness induced crack closure, explain the unusually low fatigue crack growth rates in Al–Li 2090.

5. CONCLUSIONS

The characteristic microtexture of Al–Li 2090 T8E41 that leads to the formation of asperities and crack closure in fatigue crack growth appears to be a specific type of mesotexture present in this material: sets of adjacent grains are so highly aligned that they may be regarded as nearly single crystalline volumes. A relationship between macrotexture and a specific asperity on the fatigue crack surface was identified. Thus, the size, shape and location of these asperities was shown to depend on microtexture, mesotexture, and macrotexture. When coupled with high resolution X-ray computed tomography observations of the crack face contact as a function of crack face geometry and stress intensity (in the interior of the samples) [14–17], the present observations complete the link between the orientation of individual grains/groups of adjacent grains, macro-

texture, the formation of asperities, the positions where crack faces contact as a function of applied stress and macroscopic manifestations of the crack closure process in Al–Li 2090 T8E41. Further elaboration of details such as amount and spatial distribution of near-single-crystalline regions is needed before numerically realistic models may be assayed. Fortunately gathering such information is quite straightforward with the X-ray microbeam techniques used in this work. The development of these X-ray microtexture mapping techniques is so encouraging that it is not imprudent to suggest that it should be possible to non-destructively explore the three-dimensional microtexture within intact macroscopic samples of complex materials such as Al–Li 2090.

Acknowledgements—The support of the Office of Naval Research and the encouragement of George Yoder, Office of Naval Research, are gratefully acknowledged. Experiments were preformed at SSRL, which is operated by the Department of Energy, Office of Basic Energy Sciences. Zofia Rek of SSRL is also thanked for her invaluable assistance with the microbeam experiments and R. Brown for his help with fatigue crack propagation. The authors would also like to acknowledge S. Spragg and T. Watt for their help in outputting the multitude of diffraction patterns.

REFERENCES

1. Stock, S. R., Guvenilir, A., Piotrowski, D. P. and Rek, Z. U., *MRS Symp. Proc.*, 1995, **375**, 275.
2. Piotrowski, D. P., Synchrotron polychromatic X-ray diffraction tomography of large grained polycrystalline samples. MS thesis, Georgia Institute of Technology, Atlanta, March 1996.
3. Piotrowski, D. P., Stock, S. R., Guvenilir, A., Haase, J. D. and Rek, Z. U., *MRS Symp. Proc.*, 1996, **437**, 125.
4. Stock, S. R., Haase, J. D., Piotrowski, D. P., Witt, J. R. and Guvenilir, A., Making and using small X-ray beams. Eighth Users Mtg for the Advanced Photon Source (to be published).
5. Pao, P. S., Cooley, L. A., Imam, M. A. and Yoder, G. R., *Scripta metall.*, 1989, **23**, 1455.
6. Venkateswara Rao, K. T., Yu, W. and Ritchie, R. O., *Metall. Trans.*, 1988, **19A**, 549 and 563.
7. Yoder, G. R., Pao, P. S., Imam, M. A. and Cooley, L. A., in *Proc. Fifth Int. Aluminum–Lithium Conf.*, ed. T. H. Sanders Jr and E. A. Starke Jr. Materials and Component Engineering, Birmingham, 1989, p. 1033.
8. Yoder, G. R., Pao, P. S., Imam, M. A. and Cooley, L. A., *Scripta metall.*, 1988, **22**, 1241.
9. Adams, B. L., Wright, S. I. and Kunze, K., *Metall. Trans.*, 1993, **24A**, 819.
10. Dingley, D. J., *Scanning Electron Microscopy*, 1984, **2**, 569.
11. Poulsen, H. F., Garbe, S., Lorentzen, T., Juul Jensen, D., Poulsen, F. W., Anderson, N. H., Frello, T., Feidenhans'l, R. and Graafsma, H., *J. Synchrotron Rad.*, 1997, **4**, 147.
12. Wang, P. C., Cargill, G. S. III and Noyan, I. C., *MRS Symp. Proc.*, 1995, **375**, 247.
13. Ritchie, R. O., in *Fatigue Thresholds*, ed. J. Backland, A. Blom and C. J. Beevers. Engng Advisory Services, Warley, 1981, p. 503.
14. Ritchie, R. O., *Mater. Sci. Engng*, 1988, **103**, 15.
15. Breunig, T. M., Stock, S. R., Antolovich, S. D., Kinney, J. H., Massey, W. N. and Nichols, M. C., *ASTM STP*, 1992, **1131**, 749.
16. Guvenilir, A., Bruenig, T. M., Kinney, J. H. and Stock, S. R., *Acta mater.*, 1997, **45**, 1977.
17. Guvenilir, A., Investigation into asperity induced closure in an Al–Li alloy using X-ray tomography. Ph.D. thesis, Georgia Institute of Technology, Atlanta, December 1995.
18. Guvenilir, A., Stock, S. R., Barker, M. D. and Betz, R. A., in *4th Int. Conf. on Aluminum Alloys*, ed. T. H. Sanders Jr and E. A. Starke Jr. Georgia Institute of Technology, Atlanta, 1994, p. 413.
19. ASTM Standard E-399-83.
20. Yoder, G. R., Cooley, L. A. and Crooker, T. W., in *Fatigue 84*, Vol. I, ed. C. J. Beevers, J. Backlund, P. Lukas, J. Schijve and R. O. Ritchie. Engng Advisory Services, West Midlands, 1984, p. 351.
21. Ameniya, Y., Matsushita, T., Nakagawa, A., Satow, Y., Miyahora, J. and Chikawa, J., *Nucl. Instrum. Meth.*, 1988, **A266**, 645.
22. Whiting, B. R., Owen, J. F. and Rubin, B. R., *Nucl. Instrum. Meth.*, 1988, **A266**, 628.
23. Stock, S. R., Rek, Z. U., Chung, Y. H., Huang, P. C. and Ditchek, B. M., *J. appl. Phys.*, 1993, **73**, 1.
24. Barlat, F., Miyasota, S. M., Liu, J. and Brem, J. C., in *4th Int. Conf. on Aluminum Alloys*, ed. T. H. Sanders Jr and E. A. Starke Jr. Georgia Institute of Technology, Atlanta, 1994, p. 389.
25. Suresh, S., *Fatigue of Materials*. Cambridge University Press, Cambridge, 1991, pp. 194–196.

CONCLUSIONS

A Cu/Al multilayer FZP was fabricated by use of a DC sputtering deposition process and mechanical thinning (polishing) process. During the deposition process, lower Ar gas pressure or higher rotating speed of a wire substrate has been effective in forming smoother multilayer interfaces (zones). From a focusing test of the FZP (100-zones) by the SR (8 KeV), microbeams of 1.5 μm ϕ and 0.8 μm ϕ have been achieved for the first- and third-order focal beams, respectively. The intrinsic focusing efficiencies achieved by the zoned area for the first- and third-order focal beams have been 12 % and 3 %, respectively. The focusing efficiency of the third-order focal beam has been somewhat larger than the theoretical value. Theoretically, it is one-ninth of the efficiency of the first-order focal beam. The measured focal length (141 mm, see Fig.5) was longer than the designed one. We are now investigating the reasons.

ACKNOWLEDGEMENTS

This work was performed with the approval of Photon Factory Advisory Committee (Proposal No.95G322).

REFERENCES

1. A.Snigirev, I.Snigireva, P.Engstom, S.Lequien, A.Suvorov, Ya.Hartman, P.Suvorov, P.Chevallier, M.Idir, F.Legrand, G.Soullie and S.Engrand, Rev. Sci. Instrum., **66**, 1461 (1995).
2. B.Lai, W.B.Yun, D.Legnini, Y.Xiao, J.Crzas, P.J.Viccaro, V.White, S.Bajikar, D.Denton, F.Cerrina, E.Di.Fabrizio, M.Gentili, L.Grella and M.Baciocchi, Appl. Phys. Lett., **61**, 1877 (1992).
3. D.M.Mills, J. Synchrotron Radiation, **4**, 117 (1997).
4. N.Kamijo, S.Tamura, Y.Suzuki, K.Handa, A.Takeuchi, S.Yamamoto, M.Ando, K.Ohsumi and H.Kihara, Rev. Sci. Instrum., **68**, 14 (1997).
5. Y.Suzuki, N.Kamijo, S.Tamura, K.Handa, A.Takeuchi, S.Yamamoto, H.Sugiyama, K.Ohsumi and M.Ando, J. Synchrotron Radiation, **4**, 60 (1997).
6. S.Tamura, K.Mori, T.Maruhashi, K.Yoshida, K.Ohtani, N.Kamijo, Y.Suzuki and H.Kihara in Thin Films --- Structure and Morphology, edited by S.C.Moss, D.Ila, R.C.Cammarata, E.H.Chason, T.L.Einstein and E.D.Williams (Mater. Res. Soc. Proc. **441**, Boston, MA, 1996) pp.779-784.
7. S.Tamura, K.Ohtani, N.Kamijo, T.Suzuki and H.Kihara, Thin Solid Films, **281/282**, 243 (1996).
8. J.A.Thornton, J. Vac. Sci. Technol., **A4**, 3059 (1986).
9. D.L.Windt, W.L.Brown, C.A.Volkert and W.K.Waskiewicz, J. Appl. Phys., **78**, 2423 (1995).
10. N.Kamijo, S.Tamura, Y.Suzuki and H.Kihara, Rev. Sci. Instrum., **66**, 2132 (1995).

MICRO-, MESO- AND MACRO-TEXTURE AND FATIGUE CRACK ROUGHNESS IN Al-Li 2090 T8E41

J.D. HAASE, A. GUVENILIR, J.R. WITT and S. R. STOCK
School of Materials Science and Engineering and Mechanical Properties Research Laboratory
Georgia Institute of Technology, Atlanta, GA 30332-0245

ABSTRACT

The use of synchrotron polychromatic x-ray microbeams in the transmission geometry is described for mapping grain orientation as a function of position and for relating this microtexture to the formation of large asperities on fatigue crack surfaces in Al-Li 2090 T8E41. In common with the centers of rolled plates of many aluminum alloys, Al-Li 2090 T8E41 has a sharp average texture or macrotexture different from that in the outer portions of the plate. The geometry of large asperities in Al-Li 2090 has been related to this macrotexture, and the resulting roughness-induced crack closure is recognized to be responsible for the very low crack propagation rates in certain plate orientations. This report focuses on why asperities form at certain positions and why the crack remains relatively planar elsewhere. The microtexture (i.e., the grain-to-grain orientation variation) seems to be organized into a specific type of mesotexture: multiple adjacent grains have nearly identical orientations and form substantial volumes of near-single-crystal material. Transitions between differently oriented near-single-crystal volumes or between a near-single- crystal region and more randomly oriented grains appear to bound asperities.

INTRODUCTION:

In Al-Li 2090 T8E41 fatigue crack growth rates along certain plate orientations are unusually low compared to those of other Al alloys [1,2]; very rough cracks are formed and the faces of asperities have been correlated with the strong macrotexture (i.e., the sample's average texture) in the center of the plates [3]. This crack face roughness produces crack closure, the phenomenon where the crack faces come into contact prematurely during unloading of the sample (i.e., before the minimum stress of a fatigue cycle is reached) or where the crack faces remain in contact much longer than expected during loading [4], and leads to a reduced driving "force" for crack propagation and lower fatigue crack growth rates [5]. X-ray microtomography demonstrates complex patterns of crack face contact as a function of applied load [6-10] and reinforces the view that what determines the particular crack path is the three-dimensional distribution of grain orientations, not only immediately adjacent to the crack but also in the volumes where the crack could have propagated. Recording transmission Laue patterns with synchrotron microbeams avoids the enormous effort of serial sectioning required with electron-based techniques, but very few reports of microbeam diffraction have appeared for polycrystalline materials [11-16] despite the efficiency of this approach for studying three-dimensional microtexture and its relationship to macroscopic phenomena such as fatigue crack propagation.

Mat. Res. Soc. Symp. Proc. Vol. 524 © 1998 Materials Research Society

EXPERIMENTS:

Fatigue cracks were grown in L-T oriented compact tension samples of Al-Li 2090 T8E41 (i.e., loading along the L or rolling direction and crack propagation along the plate's T or transverse direction) with R = 0 .1 (i.e., $\sigma_{min}/\sigma_{max}$), 5 Hz frequency and haversine wave form. The 2.7 mm thick compact tension samples were machined from the center of plates with scaling in accordance with ASTM E-399-83 [8, 9, 17]. After fracture, the volume of material adjacent to the crack was cut from the sample so that the specimen could be examined in the transmission parallel to the rolling direction (Fig. 1). The sample thicknesses (along L) was kept less than 3 mm because examining material within 3 mm above and below the nominal crack plane reveals the grain orientations from which the crack selected its path. One side of sample CT21 and both sides of CT11 were studied.

Polychromatic bending magnet radiation at Stanford Synchrotron Radiation Laboratory (SSRL) beamline 2-2 (3.0 GeV, beam currents between 20 and 100 mA) was used with a 10 μm diameter pinhole collimator to record the transmission Laue patterns on image storage plates [18, 19]. Data was collected on image plates, and exposures were on the order of 1 x 10^4 mA.sec. The collimator was placed 55 cm from the sample, and the beam broadened to about 80 μm vertically at the sample position (which is well-suited for mapping the ~40-50 μm thick, pancake-shaped grains). The image plates for the Fuji BAS 2500 system were read with 50 μm pixels and 256 levels of contrast, and an absorption edge filter [20] was used in some exposures to help index the diffraction streaks.

Mapping of grain orientations involved recording transmission Laue patterns with the x-ray beam along the sample's L direction (i.e., in the parallel geometry). Data collection centered on large asperities and their surroundings and, where available, the matching holes on the other crack face. The separation between sampling positions along the plate's short or S axis was chosen so that each grain would contribute to more than one diffraction pattern and ranged from 20 to 100 μm.

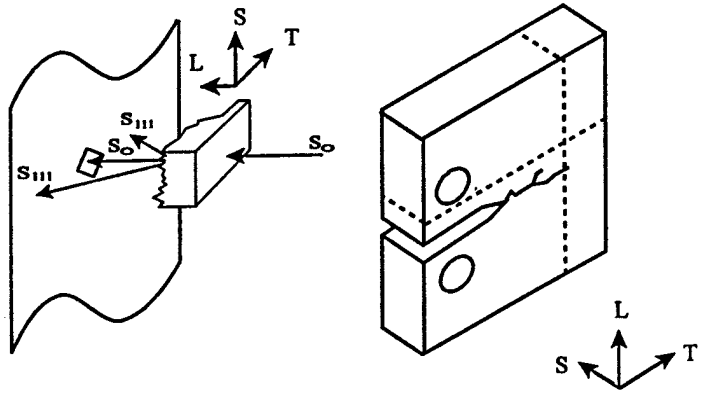

Figure 1. Geometry for recording the microbeam Laue patterns is shown on the left. The incident beam S_0 passes through the sample and strikes the beam stop while the diffracted beams S_{hkl} reach the image plate. The dashed lines (right) indicate cuts required to remove sample volumes from compact tension specimens, and the axes show the plate orientations.

RESULTS AND DISCUSSION

Microbeam diffraction reveals that the boundary between planar regions of the crack face and asperities corresponds to a specific change in orientation of grains within and outside the asperities. Figure 2 shows a typical example of this observation for sample CT21. The top pair of images show large parts of the Laue patterns from positions inside an asperity (right) and outside the same asperity (left) while the bottom pair of images show enlargements of the central part of the two patterns. The white area near the center of the pattern is the beam stop, and the dark streaks on the right-hand side are 111 "spots" from the several grains intercepted by the beam (the darker the pixel the greater the diffracted intensity). The abrupt change of texture at the edge of the asperity is seen by the quite pronounced change in 111 streak orientations. Within the asperity volume, the 111 streaks showed only minor changes from the positions shown in Fig. 2 (right), which is consistent with what is seen for other asperities. This means that multiple adjacent grains have nearly identical orientation and asperities consist of near-single-crystal material and that the presence of this type of mesotexture is important for asperity formation in Al-Li 2090 T8E41.

Figure 3 shows Laue patterns from a second orientation of near-single-crystal material: well-defined ellipses of diffraction streaks are seen, characteristic of transmission Laue patterns of single crystals. The two patterns were recorded from positions over 1 mm apart, and similar patterns appear throughout the central 3 mm thickness of plates of Al-Li 2090. Plotting the diffracted beam directions of the ellipses on a stereographic projection, and comparing the zone axis with 111, 200 and 220 pole figures reveals the zone axes to be <110>. Indices for each "spot" in a typical ellipse, consistent with the measured Bragg angle and the range of wavelengths in the polychromatic beam, are shown in Fig. 4 which

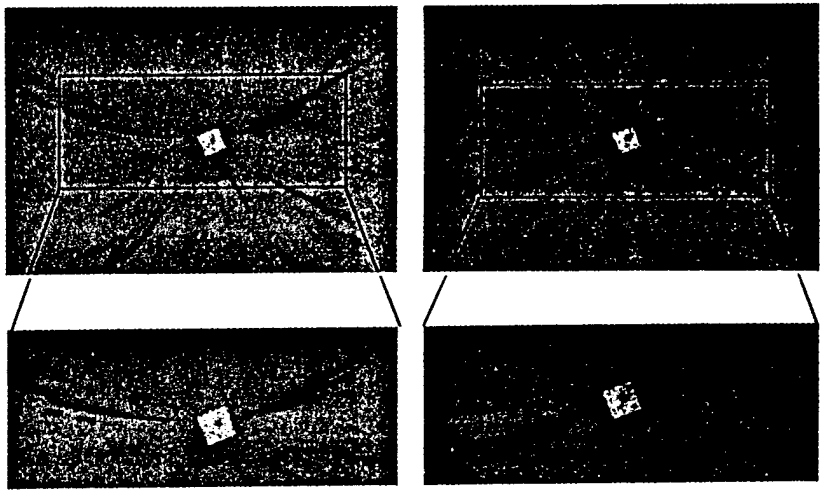

Figure 2. Transmission Laue patterns within (right) and outside (left) of an asperity. Enlargements appear below, 111 diffraction streaks are horizontal near the shadow of the square beam stop and darker pixels correspond to greater diffracted intensities.

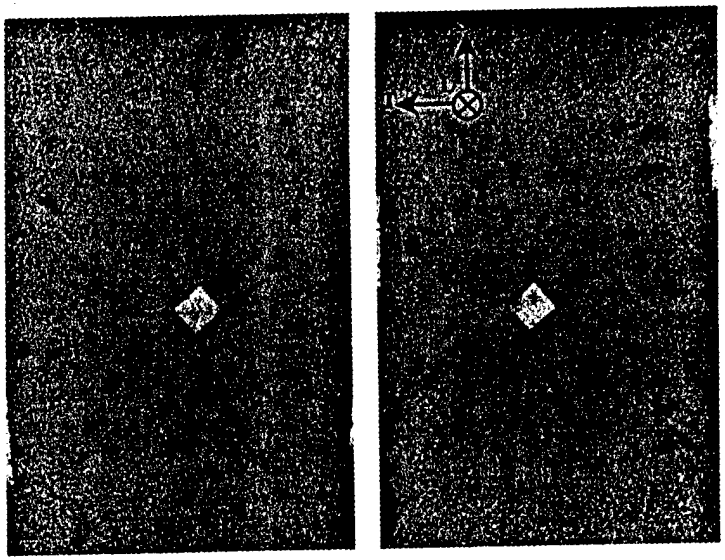

Figure 3. Diffraction patterns showing near-single-crystal volumes from two positions over 1 mm apart. The elliptical pattern of streaks are from a <110> zone, and increasing diffracted intensity is indicated by darker pixels.

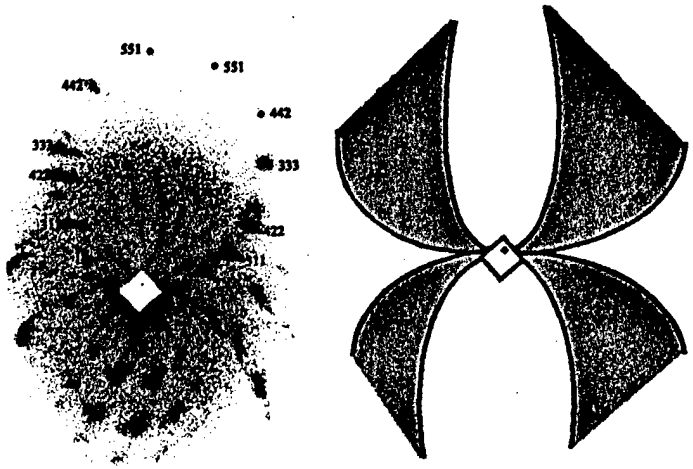

Figure 4. Indexed diffraction streaks comprising a single ellipse (left) and a schematic illustrating the range of ellipse orientations (right).

also shows the limits of the ellipses schematically. The range of ellipse orientations is consistent with the range of orientations in the 220 pole figure [3].

A consistent picture emerges of the relationship between microtexture, mesotexture, macrotexture, asperity formation and "choice" of crack path of the central portion of plates of Al-Li 2090 T8E41. Groups of adjacent, highly-oriented, pancake-shaped grains form near-single-crystal regions within the plate, approximately 45% of the plates' volumes consists of near-single-crystal regions of one orientation type or another, and this picture is consistent with the distribution of grain boundary disorientation angles measured by others [21]. Slip in Al-Li alloys is extremely planar and leads to pronounced crystallographic faceting of fracture surfaces, cracks would be expected to propagate crystallographically within or adjacent to these highly-oriented volumes and crack deflection is likely at the boundary of such a region. Normally one expects fracture feature sizes and aspect ratios similar to the grain size, but, with the pancake-shaped grains being correlated spatially and orientationally, it is not surprising that large asperities are often seen. The orientation of these near-single crystal mesotexture regions has been correlated to the macrotexture of the material and the location of these regions has also been correlated to fatigue surface features. Thus, the spatial distribution of these highly-oriented regions appears to govern whether or not asperities are present on fatigue crack surfaces in this alloy and where on the surfaces these asperities form.

CONCLUSIONS:

A characteristic mesotexture exists in the center of plates of Al-Li 2090 T8E41 and consists of sets of adjacent grains are so highly aligned that they may be regarded as nearly single crystalline volumes. Several different orientations of near-single-crystal volumes are observed, and these variants and their range of orientations are consistent with the macrotexture revealed in pole figures. It appears that a single orientation of near-single-crystal material comprises each large asperity and that large crack deflections occur in response to changes from one near-single-crystal volume to another or from a single-crystal volume to more randomly oriented material. Thus, this characteristic mesotexture, a scale of texture between micro- and macro-texture, appears as the origin of roughness-induced crack closure and extraordinarily low fatigue crack growth rates in Al-Li 2090 T8E41. It will be very interesting to see whether this mesotexture occurs in other alloy which exhibit the same macrotexture.

ACKNOWLEDGMENTS:

We gratefully acknowledge the support of the Office of Naval Research through grants N00014-94-1-0726 and -0306 and the encouragement of Dr. George Yoder, Office of Naval Research. Experiments were performed at SSRL, which is operated by the Department of Energy, Office of Basic Energy Sciences. We also thank Dr. Zofia Rek of SSRL for her invaluable assistance with the microbeam experiments and Mr. R Brown for his help with fatigue crack propagation. The authors would also like to acknowledge Ms. S. Spragg and Mr. T. Watt for their help in outputting the gigabytes of diffraction patterns leading to the observations reported in this paper.

REFERENCES:

1. K.T. Venkateswara Rao, W. Yu and R. O. Ritchie, Met Trans **19A**, 549 and 563 (1988).
2. P.S. Pao, L.A Cooley, M.A. Imam and G.R. Yoder, *Scr. Met.* **23**, 1455 (1989).
3. G.R. Yoder, P.S. Pao, M.A. Imam and L.A. Cooley, in *Proc. Fifth Int. Aluminum-Lithium Conf.*, T.H. Sanders, Jr. and E.A Starke, Jr., Eds, Mat. and Comp. Eng. Publ., Birmingham, UK p. 1033 (1989).
4. R.O.Ritchie, in *Fatigue Thresholds*, J. Backland, A. Blom and C.J. Beevers, eds., Eng Advisory Services, Warley, UK, p. 503 (1981).
5. R.O.Ritchie, *Mater. Sci. and Eng.* **103**, 15 (1988).
6. T.M. Breunig, S.R. Stock, S.D. Antolovich, J.H. Kinney, W.N. Massey and M.C. Nichols, *ASTM STP* **1131**, 749 (1992).
7. A. Guvenilir, T.M. Bruenig, J.H. Kinney and S.R. Stock, *Acta. Mat.* **45**, 1977 (1997).
8. A. Guvenilir, *Investigation into Asperity Induced Closure in an Al-Li Alloy Using X-Ray Tomography*, PhD Thesis, Georgia Inst. of Technology. December 1995.
9. A. Guvenilir, S.R. Stock, M.D. Barker, and R.A. Betz, in *4th Int. Conf. On Aluminum Alloys*, T.H. Sanders, Jr. and E.A. Starke, Jr., Eds., Georgia Institute of Technology, Atlanta, p. 413 (1994).
10. A. Guvenilir and S.R. Stock, *Fract. Fatigue Eng. Mater. Struct.*, in press May 1998.
11. S.R. Stock, A. Guvenilir, D.P. Piotrowski, and Z.U. Rek, *MRS Symp. Proc.* **375**, 275 (1995).
12. D.P. Piotrowski, *Synchrotron Polychromatic X-ray Diffraction Tomography of Large Grained Polycrystalline Samples*, MS Thesis, Georgia Institute of Technology. March 1996.
13. D.P. Piotrowski, S.R. Stock, A. Guvenilir, J.D. Haase, and Z.U. Rek, *MRS Symp. Proc.* **437**, 125 (1996).
14. H.F Poulsen, S. Garbe, T. Lorentzen, D. Juul Jensen, F.W. Poulsen, N.H. Anderson, T. Frello, R. Feidenhans'l and H. Graafsma, *J. Synchrotron Rad.* **4**, 147 (1997).
15. P.C Wang, G.S. Cargill III and I.C. Noyan, *MRS Symp. Proc.* **375**, p.247 (1995).
16. J.D. Haase, A. Guvenilir, J.R. Witt and S.R. Stock, *Acta Mat.* in press (1998).
17. ASTM Standard E-399-83.
18. Y. Ameniya, T. Matsushita, A. Nakagawa, Y. Satow, J. Miyahora and J. Chikawa, *Nucl. Instrum. Meth.* **A266**, 645 (1988).
19. B.R. Whiting, J.F. Owen and B.R. Rubin, *Nucl. Instrum Meth.* **A266**, 628 (1988).
20. S.R. Stock, Z.U. Rek, Y.H. Chung, P.C. Huang, and B.M. Ditchek, *J Appl Phys*, **73**, 1 (1993).
21. F. Barlat, S.M. Miyasota, J. Liu and J.C. Brem, in *4th Int. Conf. on Aluminum Alloys*, T.H. Sanders, Jr. and E.A. Starke, Jr., Eds., Georgia Inst. Tech., Atlanta, p.389 (1994).

X-RAY MICROBEAM QUANTIFICATION OF GRAIN SUBDIVISION ACCOMPANYING LARGE DEFORMATIONS OF COPPER

G.C. Butler[1], A. Guvenilir[2], D.L. McDowell[1,2] and S.R. Stock[2]
Mechanical Properties Research Laboratory and [1]George W. Woodruff School of Mechanic Engineering or [2]School of Materials Science and Engineering, Georgia Institute of Technology, Atlanta, Georgia 30332-0245

ABSTRACT

Polychromatic synchrotron x-ray microbeams offer a very efficient alternative to electror beam methods for quantifying the amount and character of grain subdivision accompanying large deformations. With a 0.01 mm diameter collimator, bending magnet radiation from a 3.0 GeV source and image storage plates, samples of copper with thicknesses greater than mm have been studied. Results from an as-received sample and a sample deformed to 100 torsion are compared and illustrate how efficiently grain subdivision can be quantified with polychromatic microbeam diffraction.

INTRODUCTION

Metal forming operations are often designed to produce specific types of anisotropy in gr shape, size and orientation. The pattern of preferred orientation of the grains is termed tex and can be considered to consists of three size scales. Macrotexture refers to the average texture of a sample, microtexture describes the orientation of individual grains and mesotexture denotes the orientation of ensembles of adjacent grains [1], i.e., a local averag texture. Despite experimental estimates showing that grain subdivision contributes levels o anisotropy comparable to that of grain reorientation at low to moderate strains [2], texture modeling has largely ignored this complication.

The Taylor model [3, 4] is widely used to average the response of individual grains and assumes each subunit (grain) experiences the same deformation as the aggregate. Texture prediction is often based on the Taylor model [5-7]; while this approach represents the qualitative aspects of texture distribution reasonably well, experiment shows a less sharp, n slowly developing texture than predicted [8, 9]. Treatment of grains as discrete entities largely ignores the development of substructure observed within the grains. Disorientation: greater than 10° between adjacent (~1 μm) domains are common in fcc materials after equivalent von Mises strains $\epsilon_{vM} > 1$ [10]. If the resulting spread of orientations within ea grain does not retard its net rotation, it most certainly produces less sharply defined macrotexture than would be the case if grains were regarded as monolithic entities. Thus, macrotexture does not sharpen as rapidly as predicted by grain rotation models, and it is difficult to see how models could match experiment without incorporating this effect.

Quantification of preferred orientation or macro-texture began with Wever's x-ray diffraction work [11] and still receives significant coverage in basic x-ray diffraction textbo [12, 13]. Recently, electron diffraction in transmission electron microscopy (TEM) and electron channeling or backscattering (i.e., orientation imaging microscopy or OIM [14, 15 in scanning electron microscopy (SEM) has been used in this application. Recent texture quantification emphasizes OIM for microtexture measurements used to construct macrotext pole figures [16] or for quantification of disorientations between adjacent grains [17] or TE

Mat. Res. Soc. Symp. Proc. Vol. 524 © 1998 Materials Research Society

X-RAY MICROBEAM QUANTIFICATION OF GRAIN SUBDIVISION ACCOMPANYING LARGE DEFORMATIONS OF COPPER

G.C. Butler[1], A. Guvenilir[2], D.L. McDowell[1,2] and S.R. Stock[2]
Mechanical Properties Research Laboratory and [1]George W. Woodruff School of Mechanical Engineering or [2]School of Materials Science and Engineering, Georgia Institute of Technology, Atlanta, Georgia 30332-0245

ABSTRACT

Polychromatic synchrotron x-ray microbeams offer a very efficient alternative to electron beam methods for quantifying the amount and character of grain subdivision accompanying large deformations. With a 0.01 mm diameter collimator, bending magnet radiation from a 3.0 GeV source and image storage plates, samples of copper with thicknesses greater than 0.1 mm have been studied. Results from an as-received sample and a sample deformed to 100% torsion are compared and illustrate how efficiently grain subdivision can be quantified with polychromatic microbeam diffraction.

INTRODUCTION

Metal forming operations are often designed to produce specific types of anisotropy in grain shape, size and orientation. The pattern of preferred orientation of the grains is termed texture and can be considered to consists of three size scales. Macrotexture refers to the average texture of a sample, microtexture describes the orientation of individual grains and mesotexture denotes the orientation of ensembles of adjacent grains [1], i.e., a local average texture. Despite experimental estimates showing that grain subdivision contributes levels of anisotropy comparable to that of grain reorientation at low to moderate strains [2], texture modeling has largely ignored this complication.

The Taylor model [3, 4] is widely used to average the response of individual grains and assumes each subunit (grain) experiences the same deformation as the aggregate. Texture prediction is often based on the Taylor model [5-7]; while this approach represents the qualitative aspects of texture distribution reasonably well, experiment shows a less sharp, more slowly developing texture than predicted [8, 9]. Treatment of grains as discrete entities largely ignores the development of substructure observed within the grains. Disorientations greater than 10° between adjacent (~1 μm) domains are common in fcc materials after equivalent von Mises strains $\epsilon_{vM} > 1$ [10]. If the resulting spread of orientations within each grain does not retard its net rotation, it most certainly produces less sharply defined macrotexture than would be the case if grains were regarded as monolithic entities. Thus, macrotexture does not sharpen as rapidly as predicted by grain rotation models, and it is difficult to see how models could match experiment without incorporating this effect.

Quantification of preferred orientation or macro-texture began with Wever's x-ray diffraction work [11] and still receives significant coverage in basic x-ray diffraction textbooks [12, 13]. Recently, electron diffraction in transmission electron microscopy (TEM) and electron channeling or backscattering (i.e., orientation imaging microscopy or OIM [14, 15]) in scanning electron microscopy (SEM) has been used in this application. Recent texture quantification emphasizes OIM for microtexture measurements used to construct macrotexture pole figures [16] or for quantification of disorientations between adjacent grains [17] or TEM

Mat. Res. Soc. Symp. Proc. Vol. 524 © 1998 Materials Research Society

for quantification of subgrain domain disorientations [10, 18]. Microbeam x-ray diffraction was relatively neglected, insofar as it was applied to mapping strain, microtexture, etc in polycrystalline sample, until dedicated storage rings for production of synchrotron radiation became routinely available [1, 19-22]. Mapping with 1 μm diameter or smaller microbeams is being devedloped by several groups [23, 24].

EXPERIMENTS

The samples were OFHC (oxygen-free high conductivity) Cu with an initial grain size of approximately 60 μm [25]. One sample was cut from the as-received material, a second sample was from material subjected to 50% compression, the third was from a sample subjected to 50% compression followed by 50% torsion and the fourth was from specimens strain in torsion to 100%. The thin-walled torsion specimen design, adapted from that of Lindholm et al [26], limits deformation to the gage section, even at large strains, and maintains a high degree of shear strain uniformity in this volume. The free-end torsion tests were conducted at room temperature at an effective strain rate of 4×10^{-4} s^{-1}, and 111, 200, and 220 pole figures from the samples are reported elsewhere [27] and are consistent with those reported in the literature. Planar sections of the samples were cut with a slow speed diamond wheel, were hand ground from 1 mm thick sections into wedges, were polished on SiC paper and were etched to remove polishing damage. The portion of the samples examined with the x-ray microbeam was about 100 μm and no more than 200 μm thick.

Diffraction data were collected with polychromatic bending magnet radiation at the SSRL beamline 2-2 (3.0 GeV, beam currents between 100 and 50 mA). Microbeam diffraction was performed initially with a 10 μm diameter pinhole collimator placed 55 cm from the sample; subsequently the separation was reduced to approximately 8 cm. In the former case the ~20 arcseconds of vertical divergence of the beam was enough to broaden the beam from the 10 μm diameter collimator to 80 μm vertically at the sample position [28]. Image storage plates [29,30] record the transmission Laue patterns, and both the image storage plates and the wedge-shaped samples were normal to the incident beam. Initially, 20 x 25 cm plates were read with 100 μm pixel size and 1024 levels of contrast in a Fuji BAS-2000 Imaging Plate Scanner. Once a Fuji BAS-2500 Imaging Plate Scanner became available, all data were collected on 20 x 40 cm plates and read with 50 μm pixel resolution and 256 levels of contrast. Additional levels of contrast could be obtained in the BAS-2500 system at the cost of much larger data file sizes, but 256 levels of contrast provided adequate range for these experiments. Exposures were on the order of 4×10^4 mA·sec.

Beams diffracted from the specimen passed through 3 mm of Al on the front of the holder for the image plates. A diamond-shaped, Pb beam stop was attached to the front of the plate holder, and its shadow is a prominent feature in all of the diffraction patterns. For some of the diffraction patterns, a filter with and absorption edge in the wavelength range of interest (i.e., Pd, Zr, or Mo) was placed in the incident beam to produce a sharp change in contrast in the polycrystalline diffraction pattern and to simplify indexing the diffraction pattern [31]. Wavelengths below the absorption edge were heavily attenuated while those above the absorption edge are lightly attenuated. The image plate to sample distance and the separation between the edge position and the incident beam position (i.e., where it was recorded on the image plate) were used to compute the diffraction angle for that absorption edge, and, with the wavelength and diffraction angle defined, Bragg's law was used to determine the corresponding d-spacing and hkl indices. Microtexture was mapped in the specimens by

translating the sample along the two orthogonal axes perpendicular to the beam by fixed increments (generally 10 μm) and recording the resulting transmission Laue pattern.

RESULTS AND DISCUSSION

Figure 1 compares transmission Laue patterns from the as-received copper (top left), the 50% compression sample (top right), the 50% compression-50% torsion sample (bottom left) and the 100% torsion sample (bottom right); this data was recorded with the smaller sample-collimator separation. The black circle marks the position where the azimuthal variation of diffracted intensity was measured, and wider streaks indicate greater spread of orientations associated with the irradiated volume. The background is white, with increasing diffraction intensity shown by darker pixels, Little broadening of the diffraction streaks is seen in the as-received material, more broadening is evident after 50% compression, and the two samples with 100% effective strain show the greatest azimuthal widths. Figure 2 shows the azimuthal variation of diffracted intensity, but numerical values of peak widths, etc. are not yet available. Data with the larger collimator-sample separation shows azimuthal full-widths at half maximum intensity between 2° and 5° while this quantity was between 25° and 30° after 100% torsion. Furthermore, three or more sharply-defined substreaks were within the envelope of a single streak after 100% torsion.

Figure 3 is of the 50% compression, 50% torsion sample and shows diffraction patterns recorded from four positions separated by 10 μm translations. The horizontal diffraction

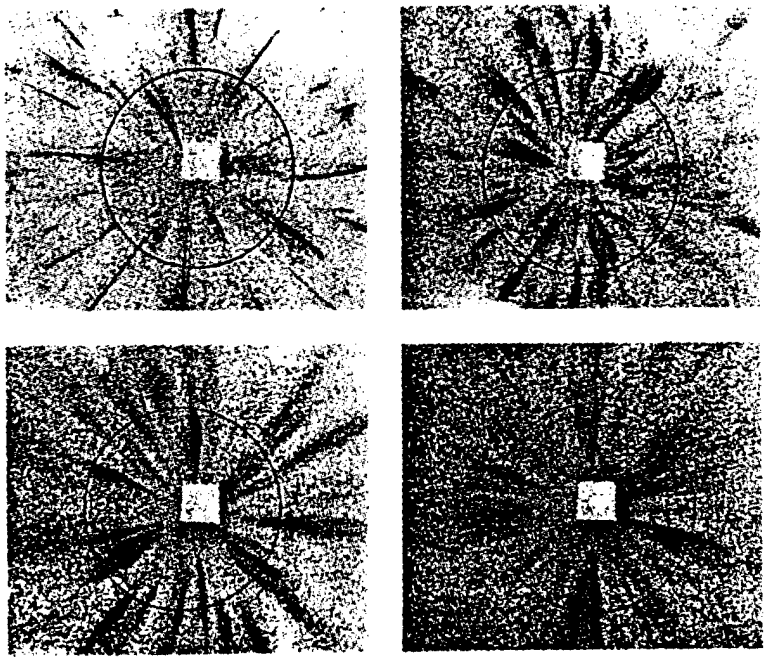

Figure 1. Transmission Laue patterns recorded with a 10 μm diameter pinhole collimator for as-received OFHC copper, after 50% compression, after 100% torsion, and after 50% compression followed by 50% torsion (clockwise from upper left). Lowest intensities are white with increasing diffraction intensity shown by darker pixels. The dark square in each is the beam stop.

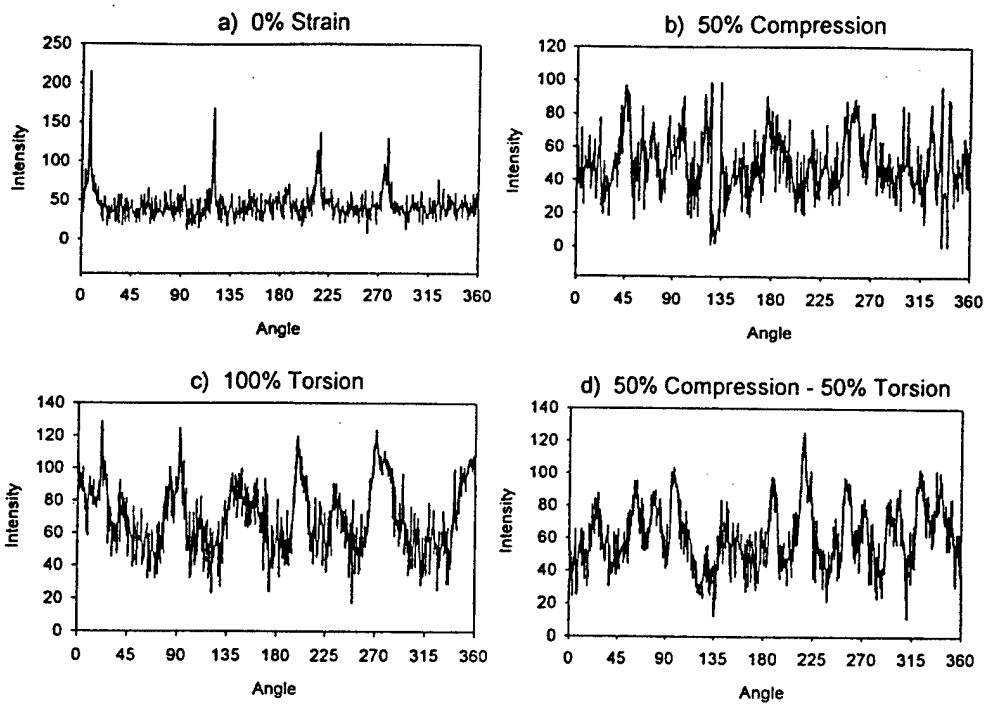

Figure 2. Azimuthal variation of diffracted intensity along the black circles shown in Fig. 1

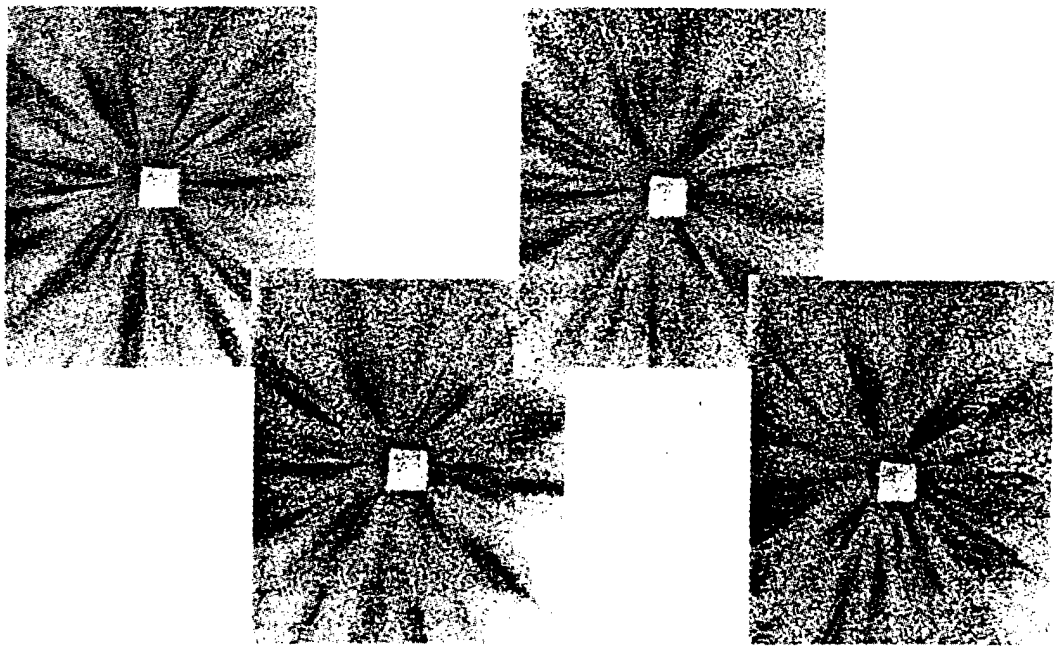

Figure 3. Laue patterns of the 50% compression, 50% torsion sample at four positions separated by 10 μm translations. The gray scale is the same as Fig. 1.

streaks just to the left of the beam stop persist between 10-30 μm; since the maximum beam dimension is between 15 and 20 μm, this demonstrates that the structure observed occurs on a length scale substantially smaller than the original ~60 μm grain size. Further analysis is underway and should provide quantitative and statistically representative data on grain subdivision processes in copper.

CONCLUSIONS

Microbeam diffraction using polychromatic synchrotron x-ray radiation was demonstrated for mapping the amount and spatial distribution of deformation at length scales substantially below that of the grains in the as-received OFHC copper material. The preliminary results for samples deformed 50% in compression, 50% in compression followed by 50% torsion and 100% torsion illustrate how grain subdivision can be quantified in relative thick samples requiring little in the way of sample preparation. Even at this early stage of analysis, the results show that the spread in macrotexture observed in pole figures is due to grain subdivision processes. It is not surprising that model based on grains as the fundamental unit of crystallographic orientation predict too rapid and too sharp texture for heavily deformed samples.

ACKNOWLEDGMENTS

We thank Mr. S. Graham, Jr. of the MPRL for conducting the deformation experiments and Dr. Z.U. Rek of SSRL for her assistance. The data were recorded at SSRL which is supported by the Department of Energy. We are also grateful for the support from the Office of Naval Research (through grants N00014-94-1-0306 and -0726) and from the Army Research Office (through grants DAAH0493G00138 and DAAH049510177).

REFERENCES

1. J.D. Haase, A. Guvenilir, J.R. Witt and S.R. Stock, Adv X-Ray Anal **41** (1998) in press.
2. N. Hansen and D. Juul Jensen, Acta Mater **40** (1992) 3265.
3. G.I. Taylor, J Inst Metals **62** (1938) 307.
4. G.I. Taylor, in Steven Timoshenko 60th Anniv. Vol., Ed. J.M. Lessels, 1938, p.218.
5. R.J. Asaro and A. Needleman, Acta Metall **33** (1985) 923.
6. K.K. Mathur and P.R. Dawson, Int J Plasticity **5** (1989) 67.
7. S.R. Kalidindi and L Anand, in Adv. In Finite Deformation Prob. In Mater. Processing Structures, AMD **125** N. Chandra, J.N. Reedy, eds, ASME, 1991, p.3
8. N. Hansen and D. Kuhlman-Wilsdorf, Mater Sci Eng **81** (1986) pp. 141-161.
9. M.G. Stout, J.S. Kallend, U.F. Kocks, M.A. Przystupa and A.D. Rollet, in Proc. 8th Conf. On Textures of Mater. (ICOTOM 8), eds J.S. Kallend and G. Gottstein, TMS, 1988, p. 479.
10. D.A Hughes and N. Hansen, Acta Mater **45** (1997) 3871.
11. F. Wever, Z Phys **28** (1924) 69.
12. B.D. Cullity, Elements of X-ray Diffraction, Second Ed. Addison-Wesly, 1978.
13. C.S. Barrett and T.B. Massalski, Structure of Metals, Third Ed., Pergamon, 1986.
14. D.J. Dingley, Scanning Electron Microscopy **2** (1984) 569.

15. V. Randall, Microtexture Determination and its Applications. Inst. Metals, 1992.
16. B.L. Adams, S.I. Wright and K. Kunze, Met Trans. **24A** (1993) 819.
17. K. Matsumoto, T. Shibayanagi and Y. Umakoshi, Acta Mater **45** (1997) 439
18. D.A. Hughes, Q. Liu, D.C. Chrzan and N. Hansen, Acta Mater **45** (1997) 105
19. S. Stock, G.E. Ice, A. Habenschuss and C.J. Sparks, Jr., National Synchrotron Light Source Annual Report 1986, BNL 52045, p 354.
20. R. Rebonato, G.E. Ice, A. Habenschuss, and J.C. Billelo, Phil Mag **A60** (1989) 571.
21. G.E. Ice, Summarizing [19 and 20] in Nucl Instrum Meth **B24-25** pt. 1 (1987) 397.
22. J.D. Haase, A. Guvenilir, J.R. Witt and S.R Stock, Acta Mater in press (1998).
23. P.C. Wang, G.S. Cargill, III, and I.C. Noyan, Mat Res Soc Proc **375** (1995) 247.
24. H.F. Poulsen, S. Garbe, T. Lorentzen, D. Juul Jensen, F.W. Poulsen, N.H. Andersen, T. Frello, R. Feidenhans'l and H. Graafsma, J Synch Rad **4** (1997) 147.
25. S. Graham Jr., "The Stress State Dependence of Finite Inelastic Deformation Behavior of F.C.C. Polycrystalline Materials," M.S. Thesis, Georgia Inst. Technology, 1995.
26. U.S. Lindholm, A. Nagy, G.R. Johnson and J.M. Hoegfeldt, ASME J Eng Mater Tech **102** (1980) 376.
27. G.C Bulter, S. Graham, D.L. McDowell, S.R. Stock and V.C. Ferney, ASME J Eng Mater Tech in press (1998).
28. S.R. Stock, M.A. Langoy and R. Morano, unpublished data, December 1997.
29. Y. Ameniya, T. Matsushita, A. Nakagawa, Y Satow, J. Miyahora, and J. Chikawa, Nucl Instrum Meth. **A266** (1988) 645.
30. B.R. Whiting, J.F. Owen and B.R. Rubin Nucl Instrum Meth A266 (1988) 628.
31. S.R. Stock, Z.U. Rek, Y.H. Chung, P.C. Huang, and B.M. Ditchek, J Appl Phy **73** (1993) 1.

Jake D. Haase,[1] *Abbas Guvenilir,*[1,2] *Jason R. Witt,*[1] *Morten A. Langøy,*[1,3] *and Stuart R. Stock*[1,4]

Microtexture, Asperities, and Crack Deflection in Al-Li 2090 T8E41

REFERENCE: Haase, J. D., Guvenilir, A., Witt, J. R., Langøy, M. A., and Stock, Stuart R., **"Microtexture, Asperities, and Crack Deflection in Al-Li 2090 T8E41,"** *Mixed-Mode Crack Behavior, ASTM STP 1359,* J. Miller and D. L. McDowell, Eds., American Society for Testing and Materials, West Conshohocken, PA, 1999, pp. 000–000.

ABSTRACT: Roughness-induced closure is held to be responsible for very low fatigue crack growth rates observed in certain plate orientations of Al-Li 2090 T8E41, and the geometry of asperities producing this closure correlates with macrotexture. Little work, however, has focused on the role of individual grain orientations (microtexture) or of average orientation within small groups of adjacent grains (mesotexture) on the crack's path through a sample, i.e., on whether the variation in grains' orientations determines where the crack will deflect. This paper reports synchrotron x-ray microbeam diffraction mapping of the three-dimensional microtexture in samples of Al-Li 2090. Groups of adjacent pancake-shaped grains are found to have very similar orientations, producing nearly single-crystal regions approaching thicknesses of 0.3 mm along the sample's S (short-transverse) direction. These near-single-crystal volumes produce large asperities with surfaces having substantial Mode III character, asperities which appear over the range of stress intensity ranges observed (~5 to ~25 MPa$\sqrt{m}$). Results of these experiments suggest not only that this type of mesotexture plays an important role in determining fatigue crack path in compact tension samples of Al-Li 2090 but also that specific orientations of the groups of grains lead to large crack deflections.

KEYWORDS: crack closure (roughness-induced), fatigue, synchrotron radiation, aluminum, texture (micro-), (meso-), (macro-), x-ray diffraction (microbeam), Laue patterns, mixed-mode crack surfaces

Different scales of texture, such as macrotexture (average texture within the entire sample), microtexture (the crystallographic orientation of individual grains), and mesotexture (texture within groups of adjacent grains) can contribute to a polycrystalline material's response to deformation. In Al-Li 2090 T8E41, fatigue crack growth rates for certain plate orientations are unusually low compared to those of other Al alloys [*1–3*], and this results from sharply-defined macrotexture in the center of the plates that produces a rough, asperity-dominated crack face and significant crack deflection [*2*]; the role of micro- and meso-texture, however, appears to have received little attention. Understanding how micro- and meso-texture (particularly the size, spatial distribution, and orientation of near-single-crystal regions) affects fatigue crack paths in Al-Li 2090 T8E41 is the goal of the work described below.

[1] School of Materials Science and Engineering, Georgia Institute of Technology, 778 Atlantic Drive, Atlanta, GA 30332-0245.
[2] M/D K-10 Yield Enhancement Technology Transfer, Motorola, 3501 Ed Bluestein Blvd., Austin, TX 78721.
[3] Kvaerner Oil and Gas, Stavanger, Norway.
[4] Author to whom all correspondence should be addressed: stuart.stock@mse.gatech.edu.

Previously developed SEM (scanning electron microscopy) methods for measuring microtexture such as Orientation Imaging Microscopy (OIM) [*4,5*] are limited by their relatively shallow interaction volume that requires destructive serial sectioning for three-dimensional measurements and careful removal of polishing damage. In contrast, x-ray microbeam methods allow millimeter thicknesses to be probed quickly and nondestructively, an important advantage if the different texture scales are to be measured before crack propagation has occurred.

To this end, transmission Laue patterns using synchrotron x-ray microbeams were used to characterize the micro- and meso-texture present in the sample and how the characteristics of these different texture scales affect the crack path geometry: the approach is to determine where and how microtexture and mesotexture change relative to crack face features.

Background

One result of the crack roughness in Al-Li 2090 is crack closure, the phenomenon where the crack faces come into contact prematurely during unloading of the sample (meaning before the minimum stress of a fatigue cycle is reached) or where the crack faces remain in contact much longer than expected during loading [*6*]. Crack closure leads to a reduced driving "force" for crack propagation and lower fatigue crack growth rates [*7*], and macroscopic measurements [*1–3*] and high resolution x-ray computed tomography [*8–13*] have detailed the effect of closure in producing the very low crack growth rates in the L-T orientation of Al-Li 2090 T8E41.

In 12.7-mm-thick plates of Al-Li 2090 T8E41, the macrotexture in the center is very different from that in the outer sections [*3,14*], and the surfaces of fatigue cracks are much rougher, with larger, steeper asperities in the center. Side grooves can minimize crack deflection, but asperities with surfaces having very prominent Mode III components form nonetheless. Otherwise very large macroscopic crack deflections are the rule; these surfaces can have mixed I-III and I-II character. The center region texture consists of two strong preferred orientations {123}⟨634⟩ and {110}⟨112⟩ and one weak preferred orientation {112}⟨111⟩; and Yoder et al. [*14*] have determined that the angle between the two faces of large asperities corresponds to that between high density {111} orientations in the pole figure.

Given that the morphology of the crack surface relates to the macrotexture present, the question remains whether asperities in the center of plates of Al-Li 2090 form at random within the volume of material through which the crack is constrained to grow (by the notch) or whether variations in micro- and meso-texture within this volume dictate where large and small asperities develop. If the latter is the case, does the crack choose its path to avoid grains or groups of grains with certain orientations or to grow through individual grains, groups of grains or grain boundaries with specific orientations. Because it is unlikely that a propagating crack will always find grains oriented to provide its preferred path, the actual path will undoubtedly include grains less ideally oriented. Thus, by comparing the actual crack path with the crystallographic orientations of grains in the volume of material through which the crack might have chosen to propagate, there is an opportunity to study the interplay between what some workers call the "forcing function" and the grain orientations.

Experiments

The samples were 2.7-mm thick and were machined from the center of 12.5-mm-thick plates of Al-Li 2090 T8E41; across the sample thickness there were on the order of 50 pancake-shaped grains with dimensions ~0.05 by ~0.5 by ~1 mm along the plate's short-transverse (S), transverse (T) and rolling (L) directions, respectively. The composition (wt.

%) of the material has been reported as: 1.9-2.6 Li, 2.4-3.0 Cu, 0.08-0.15 Zr, 0.25 max Mg, 0.05 max Mn, 0.15 max Ti, 0.12 max Fe, 0.01 max Si, bal. Al [15]. The material was heat treated to peak-aged condition, and T8E41 describes the following processing steps: 549 C solution treatment, water quench, 6% stretch and 163 C age for 24 h. Mechanical properties for Al-Li 2090 T8E41 are reproduced in Table 1 [15,16]; with the large difference in K_{Ic} values for the various orientations, it is not surprising that the fracture surface morphology is so anisotropic. The threshold stress intensity range for fatigue crack growth in the L-T orientation is ΔK_{th} = 3.86 MPa$\sqrt{m}$, and K_{cl}/K_{max} = 0.86, where K_{cl} is the stress intensity factor where crack closure is observed macroscopically and K_{max} is the maximum K of the cycle in which K_{cl} is reported.

Compact tension samples were examined so that the results could be related to those of other investigators. The specific specimen dimensions are discussed elsewhere [11], but the scaling was in accordance with the ASTM Standard Test Method for Plane-Strain Fracture Toughness of Metallic Materials E-399-83 (31.8-mm length and 30.5-mm width). Fatigue cracks were grown in L-T oriented compact tension samples (meaning loading along the L direction and crack propagation along the T direction) with R = 0.1 (meaning $\sigma_{min}/\sigma_{max}$), 5 Hz frequency and haversine wave form. The samples had side grooves that minimized crack deflection and allowed valid comparisons to be made with others' observations of stress intensity range, etc.

All diffraction data were collected with polychromatic bending magnet radiation at Stanford Synchrotron Radiation Laboratory (SSRL) beamline 2-2 (3.0 GeV, beam currents between 20 and 100 mA). A pinhole collimator with 10 μm diameter was used to form the microbeam, and the collimator was placed 55 cm from the sample. The ~20 arcseconds of vertical divergence broadened the beam to ~80 μm at the sample position. Image storage plates [17,18] were used to record the Laue patterns, and the 20 by 40-cm plates were read with 50 μm pixel resolution and 256 levels of contrast on a Fuji BAS-2500 scanner. In some of the patterns, a filter with an absorption edge in the wavelength range of interest was placed in the beam before the collimator in order to introduce a sharp change in contrast in the polycrystalline diffraction pattern [19]. The known wavelength of the absorption edge allows the d-spacing (and hkl) of each spot to be determined via Bragg's law. Exposure times without the filter were 2-10 by 10^3 mAsec and depended on the beam current (total exposure equals the product of the exposure time and the x-ray beam intensity which is linearly proportional to the beam current that decays with time during a single fill of the ring). With the filter in place exposure times were approximately three times longer.

TABLE 1—*Mechanical and fatigue properties of Al-Li 2090 T8E41, where σ_y is the yield stress and UTS is the ultimate tensile stress along the* L *direction and* K_{Ic} *is the Mode I fracture toughness. The values are from* [16] *unless two values are listed; in that case the first is from* [16] *and the second from* [15].

MPa	Orientation	MPa$\sqrt{m}$
σ_y 552, 517	K_{Ic} L-T	36
UTS 583, 554	T-L	24
	T-S[b]	65
% elongation[a] 9.3, 8	S-L	17
	S-T	16

[a] In 25-mm gage.
[b] Not meeting ASTM E399 plane strain thickness requirement.

Two diffraction geometries were used (Fig. 1). The "parallel" geometry positioned the incident x-ray beam parallel to the rolling direction L (Fig. 1*a*). This geometry was suitable only for ~3-mm thick sections cut from the compact tensions samples, and the samples described below included the fracture surface as one of the faces. The "perpendicular" geometry, where the short rolling direction S and incident beam are parallel, was used both on unfractured and fractured compact tension samples (Fig. 1*b* and *c*).

Microtexture in various compact specimens was mapped by translating the sample along the two orthogonal axes perpendicular to the beam by fixed increments and recording the resulting transmission Laue patterns. Prior to microbeam data collection, the fracture surfaces were mapped with optical microscopy so that microtexture mapping could concentrate on asperities and other features of interest. For the fractured compact tension specimens, most of the Laue patterns were recorded in the parallel geometry: the beam was translated in short steps along the S direction for various positions along the T axis. The separation between sampling positions along the S axis was chosen so that diffraction features from each grain would be present in more than one diffraction pattern (to reveal gradual changes in microtexture or mesotexture) and ranged from 20 to 100 μm. The fractured compact tension specimens were also examined in the perpendicular geometry in order to assess whether asperities could be located in unfractured, unsectioned compact tension specimens.

A topographic map of one of the surfaces was made from a through focus series of micrographs (meaning micrographs were taken as the focal plane was moved in discrete increments and the regions in the micrograph that were in focus at each level were recorded) in order to identify important features on the fracture surface. Matching locations on each face of the fracture surface were studied, and the resulting diffraction patterns were compared.

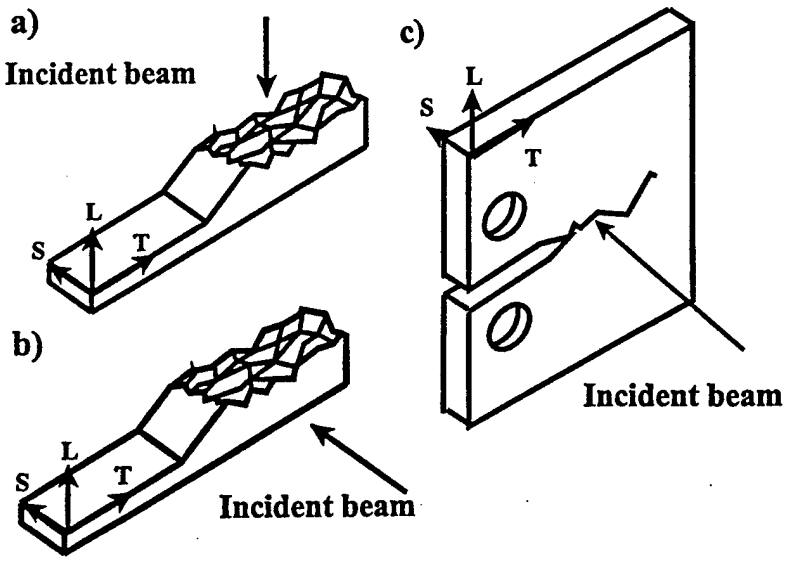

FIG. 1—*Diagram* a *shows the parallel diffraction geometry for the fractured compact tension samples: the incident beam is parallel to the rolling direction (L). In* b, *the perpendicular geometry, the beam is parallel to the short direction (S), perpendicular to the faces of the plate. Diagram* c *shows the perpendicular diffraction geometry for the unfractured compact tension samples.*

S_
N_

Results and Discussion

The anisotropic morphology of the rolled grains causes a distinct change in what is observed in Laue patterns between parallel and perpendicular geometries. Since the grain size in Al-Li 2090 along the L direction is on the order of 1 mm and along the S direction is on the order of 50 μm, diffraction patterns recorded in the parallel geometry would be expected to consist of ellipses and streaks from up to about ten grains, but not several tens of grains. In the perpendicular geometry, approximately 50 grains were traversed in the complete compact tension sample, and large numbers of streaks complicate analysis because of the grouping and overlapping nature of the streaks produced by adjacent, similarly oriented grains. Asperities appear, in one sample or another, over the range $5 < \Delta K < 25$ MPa$\sqrt{m}$, and their formation does not appear to be tied to any particular values of ΔK.

The first sample under investigation, CT21, was one side of a fractured compact tension sample. The sample, containing one fracture surface was cut in half, along a plane perpendicular to the crack propagation direction, through a prominent fracture surface asperity located next to side groove. The end including the notch was designated CT21A and the other half CT21B. Figure 2 shows a large asperity (approximately 6.5 mm from the notch tip) on sample CT21A viewed at a large angle of tilt and the center portion of diffraction patterns recorded at four positions. The white dashed line indicates the position of a scan of the beam along the sample's S direction, the large asperity is at the top of the SEM micrograph, and the arrows indicate the position where each of the four diffraction patterns were recorded. The abrupt change of texture at the edge of the asperity is seen by the quite pronounced change in streak orientations to the right of the beam stop. The patterns from the asperity (top and middle right) show steaks oriented from 3 to 4 o'clock, with the longest and most intense streak being at 4 o'clock, while the patterns outside the asperity show differently oriented streaks, such as the streaks between 2 and 3 o'clock orientation in the bottom right pattern of Fig. 2. Patterns recorded with the absorption edge filter in the beam revealed that the streaks were from 111 diffraction planes.

Figure 3 shows the same streak orientations for an interior asperity (approximately 13 mm from the notch tip) located in sample CT21B. Within the volume of the asperities, the orientation of the 111 streaks varied little from the upper pattern of Figs. 2 and 3. Outside the apserities, the 111 streaks had either different orientations or were not present. Observation of this kind of microtextural variation in multiple asperities at different positions relative to the sample's faces confirms that these features are not accidental, but rather are intrinsic to the material.

Diffraction patterns covering the asperity (located ~6.5 mm from the notch tip) in sample CT21A were also recorded in the perpendicular geometry and revealed 111 streaks that were nearly horizontal on both sides of the beam stop (at 3 and 9 o'clock positions). The results confirmed that the grains comprising the asperity were nearly identically oriented and demonstrated that the microtexture producing the 111 streaks parallel to or nearly parallel to the plate's T direction in the parallel diffraction orientation also can be unambiguously seen in the perpendicular geometry as horizontal 111 streaks. It is likely, therefore, that volumes of material with the proper microtexture to form asperities can be located nondestructively in samples prior to crack growth. Whether or not such volumes of material actually form asperities or significant crack deflection, however, depends on many other factors, including whether the advancing crack will intersect the volume.

It is also important to ascertain whether the microtexture inside and outside of the asperity described above is consistent with the expected average texture (meaning macrotexture). Figure 4 shows an experimental 111 pole figure (after Ref. *14*) from the central portion of plates of Al-Li 2090 T8E41, and the solid rectangle in the right portion of the pole figure

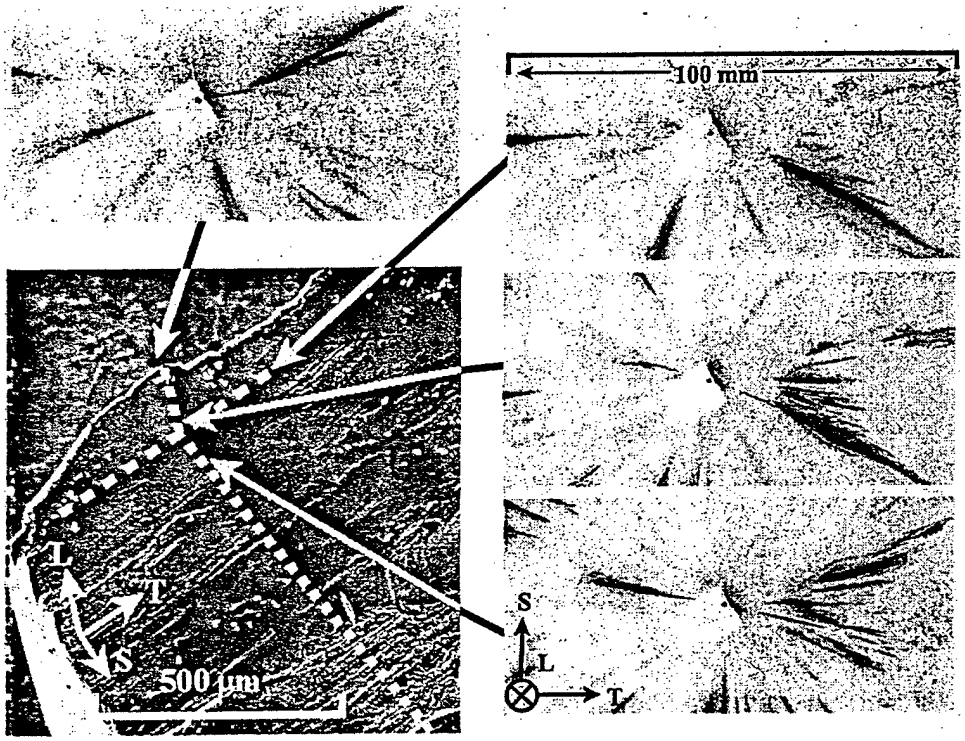

FIG. 2—*SEM fractograph of compact tension sample CT21A. The large asperity appears at the top, and the dashed line marks where the x-ray microbeam was scanned. The central portion of the diffraction patterns just within (top and middle right) and just outside (top left and bottom right) the asperity are also shown; arrows to positions on the fractograph identify where the patterns originated. The darker the pixel in the diffraction patterns, the greater the diffracted intensity. The change in streak position is characteristic of the change in microtexture seen in asperities. The image plate to detector separation was 245 mm, and the scale marker on one of the diffraction patterns shows 100 mm on the image plate.*

space not hyphen

is an idealized representation of orientations comprising one portion of the macrotexture. Comparing the orientation of the streaks observed in the parallel geometry Laue patterns with the expected exit beam directions S_{111} for the sample's macrotexture, requires that the orientation of the pole figure to be changed so that L and S_0 lies at the center of the stereographic projection (bottom pole figure). (Those without experience manipulating stereographic projections are referred to Ref. *20*.) Bragg's law requires that the entrance and diffracted beams (S_0 and S_{111}, respectively) are coplanar with and at an angle $\pi/2 - \theta_B$ from the plane normal. The end points of the two dashed lines represent the limits of the exit beam directions that would be seen from the idealized component of macrotexture; and these are represented by the narrow triangles pointing to the right from S_0. Orientations between these two would also be expected. From this representation of the macrotexture, one expects 111 streaks to be at an angle no greater than ±25° from T; experimentally the angles are ~20° up in the lower right pattern and ~25° down in the middle left pattern of Fig. 2.

In the course of developing a method to measure microtexture nondestructively in Al-Li 2090 T8E41, large groups of adjacent grains were discovered with similar orientations. Figure 5 shows the two kinds of diffraction patterns typically produced by these regions in the

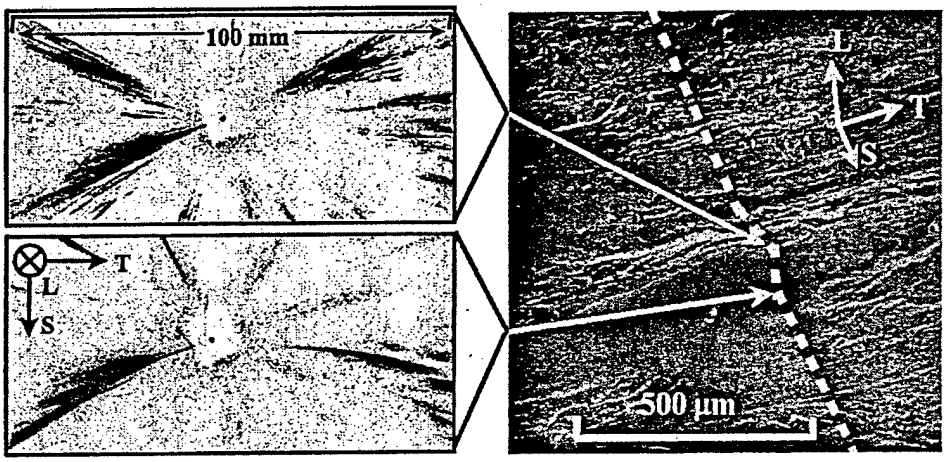

FIG. 3—*SEM fractograph of an interior asperity on sample CT21B. This figure is analogous to Fig. 2 but was recorded on an asperity far removed from the side grooves. One face of the asperity is quite shear face and may be a delamination along a grain boundary.*

parallel beam geometry. The right-hand pattern shows an elliptical arrangement of streaks (or groups of streaks), characteristic of transmission Laue patterns of single crystals, while the left-hand pattern shows arc-shaped groups of diffraction streaks. Above each of the patterns is a magnified image of one group of streaks. In the left-hand magnified image, the spots are from six distinct but nearly identically oriented grains within the column of material irradiated by the microbeam. The slight disorientations between each grain are produced by rotation about the plate's L direction, that is, the incident beam direction.

A second fractured compact tension sample, CT11, was also examined; both sides of the fracture surface were available. Two series of diffraction patterns taken along the *S* direction of this sample are shown in Fig. 6; the spacing between exposures was 50 μm. The top row of patterns (*a–d*) is clearly from a near-single-crystal region oriented to produce ellipses, and the bottom row of patterns (*e–h*) shows characteristic 111 streaks (in the middle of the pattern, to either side of the beam stop) from near-single-crystal material within an asperity. Several other locations on the fracture surface produced similar diffraction patterns: ellipse-type patterns from one side and characteristic 111 streaks along the T direction from the opposite side.

Understanding the specifics (such as misorientation angle, size, spatial distribution, etc.) of these regions of similarly aligned crystals should shed light on the effect they have on crack propagation. First, about 45% of the nonoverlapping diffraction patterns revealed near-single-crystal volumes. Consequently, the center of plates of Al-Li 2090 T8E41 can be thought of as a composite of near-single-crystal-volumes. Second, a large number of elliptical streak patterns were observed whose orientations differed little from that seen in Fig. 6*a–d*. In Fig. 7, elliptical patterns of streaks are shown schematically: the centroids of each group of streaks comprising a given pattern are represented by the same symbol. Within this near-single-crystal volume, the orientations varied by a rotation of about 12° about the incident beam across the total 400 μm of beam translation.

The orientation of near-single-crystal volumes should correspond to important components of the macrotexture, and this was checked using a stereographic projection to find the zone axis for the diffraction planes producing the individual spots of each ellipse. The zone axes

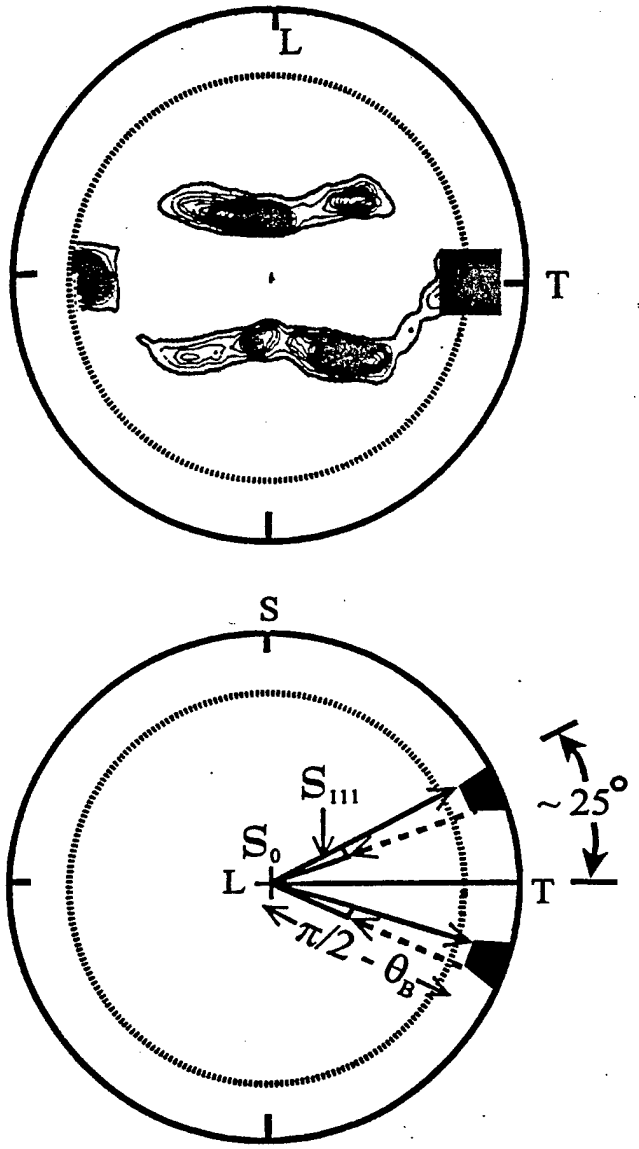

FIG. 4—*Orientation of 111 diffraction streaks related to the macrotexture of the center of plates of Al-Li 2090 T8E41. The 111 pole figure (after Ref. 14) is shown at the top, and the portion of macrotexture producing the 111 streaks associated with the asperities shown in Fig. 2 and 3 is represented schematically by the solid rectangle in the right half of the pole figure. The L-oriented stereographic projection (lower) is used to relate experimentally observed 111 streaks to the macrotexture: the locus of expected diffracted beam directions (i.e., the streaks) from the orientations within the solid rectangle are indicated by the elongated triangles extending from the L direction nearly parallel to the T axis.*

S_
N_

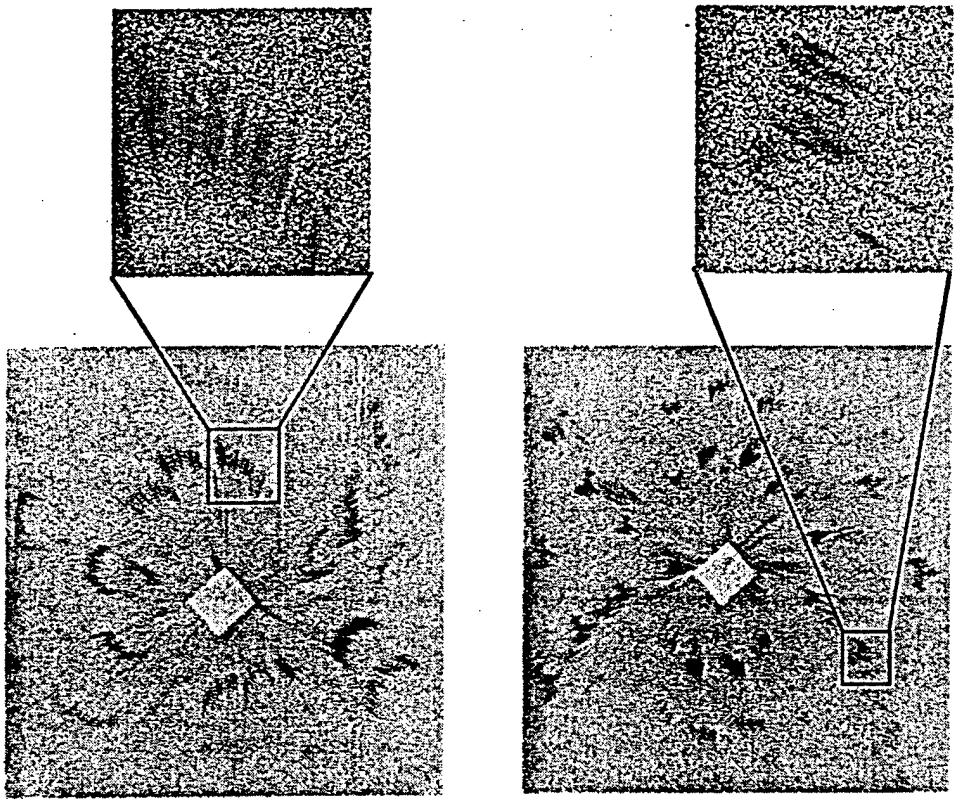

FIG. 5—*Typical transmission Laue patterns from near-single-crystal volumes exhibit patterns with either ellipses (left) or arc-shaped spots (right). Magnified views of each type of groups of spots appear above each pattern. The arrangement of these groups of spots yields information about both the orientation and arrangement of individual grains within a near-single-crystal volume. Darker pixels represent greater diffracted intensity.*

of ellipses, such as those shown in Fig. 7, were determined to be ⟨110⟩, the exact location of each ⟨110⟩ zone axis was plotted for each ellipse, and the range of locations for these normals fell within regions of high pole density in the 220 pole figure for this alloy. Figure 8 shows the orientation of ⟨110⟩ zone axis related to the macrotexture of the center of plates of Al-Li 2090. The 220 pole figure [*14*] is shown at upper left of this figure, the angular limits of the macrotexture producing the ⟨110⟩ ellipses are represented by the A and B arrows in the lower pole figure and diffraction patterns representing the limits of orientation, meaning A and B, appear to the right of the pole figure. The angular range of the ⟨110⟩ poles producing the ellipses is ~25° in the 220 pole figure. Although the range of ellipse orientations was 12° across a single near-single-crystal region, the overall range across the entire sample was ~25°, in good agreement with the 220 pole figure. Measurements of the distribution of grain boundary disorientation angles in Al-Li 2090 T8E41 [*21*] are also consistent with existence of the near-single-crystal volumes and the range of ellipse orientations observed in the diffraction patterns described above.

S_
N_

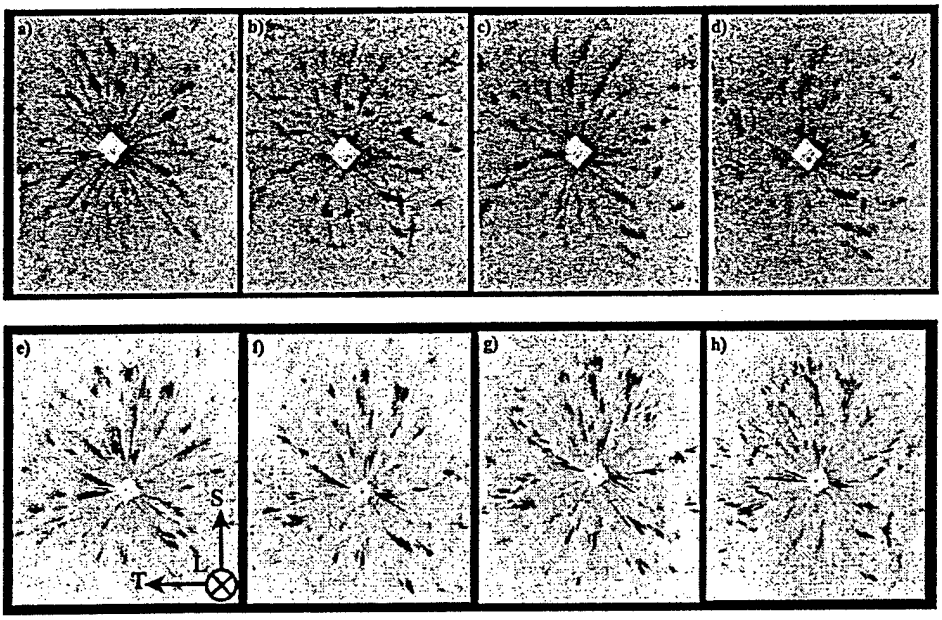

FIG. 6—*Two series of diffraction patterns that show the extent of two near-single-crystal volumes within CT11. The images were from positions 50 μm apart along the short rolling direction (S) and were recorded in the parallel geometry. The ~~top~~ row of patterns show the 111 streaks from an asperity, and the ~~bottom~~ row shows ellipse patterns from the crack face opposite the asperity.*

bottom

top

The results point to the importance of an intermediate scale between micro- and macrotexture in the "choice" of crack path of the central portion of plates of Al-Li 2090. Groups of ~5–20 adjacent, highly-oriented, plate-like grains form near-single-crystal regions within the plate, and this specific type of mesotexture defines favored crack paths. Numerous studies have demonstrated that deformation is highly planar in Al-Li alloys and that such deformation morphology leads to considerable crystallographic faceting of fracture surfaces [22]. With little change in orientation across grain boundaries within a near-single-crystal volume, it would not be surprising for a crack to propagate across the entire volume crystallographically and for large asperities to form with a geometry consistent with the sample's macrotexture. The data presented above demonstrate that the orientation of these near-single-crystal regions correlates with the macrotexture of the material and that the location of these regions is associated with specific features of fatigue crack surface. Thus, the spatial distribution of these highly-oriented regions appears to govern whether or not asperities are present on fatigue crack surfaces in this alloy/heat treatment and where on the surfaces these asperities form.

The asperities, shown above to be meso-texture-related, add a strong Mode III character to the fracture surface, and contact on the strongly mixed I-III Mode surfaces has been implicated in numerous studies as producing the extraordinarily low crack growth rates of Al-Li 2090 T8E41 samples. Mixed Mode I-II regions of the sample are also present, but these lead to large deflections of the crack that are generally visible on the sample surface; these cracks provide invalid data from an ASTM standards perspective and such data is generally discarded by investigators. The data from these inconvenient samples should not

S_
N_

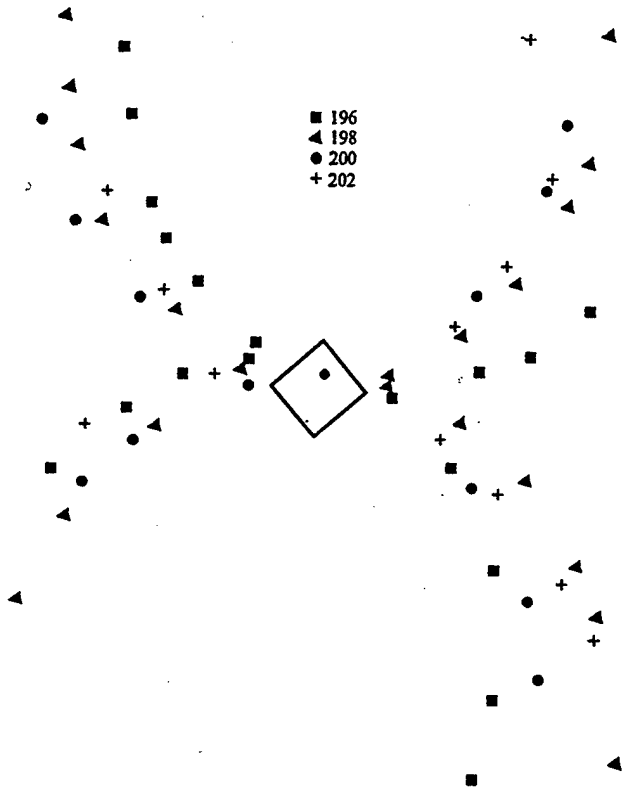

FIG. 7—*A schematic showing the orientations of adjacent near-single-crystal volumes producing ellipse patterns. The centroids of the spots of an ellipse are represented by a single symbol. Patterns from five positions spaced 100 μm apart are superimposed, and the tight grouping of symbols from different ellipses illustrates the extent of near-single-crystal volumes.*

be discarded; instead the samples should be examined closely because the large crack deflections (mixed mode surfaces) must reflect domination of metallurgical factors (mesotexture seems likely) over "forcing function" considerations. Work of this type is currently underway using the microbeam techniques employed here.

The very low fatigue crack growth rate of Al-Li 2090 in the L-T orientation is affected by the nature of the deformation in this alloy and the magnitude of crack path deviations. In samples that crack crystallographically and that have randomly-oriented grains or with poorly defined mesotexture, the magnitude of crack path deviation from the nominal crack plane would be expected to be near that of the grain size. However, in the center of plates of Al-Li 2090, the near-single-crystal mesotexture allows the crack to extend crystallographically across multiple grains and thereby to form large asperities. Given that crystallographic fatigue crack propagation is quite slow compared to other modes [*23*], large crystallographic faces in a sample would be expected to correlate with slow crack growth rates.

A second factor identified by others as slowing the crack comes from roughness-induced closure, itself a product of the mesotexture in this alloy. In situ, high resolution x-ray computed tomography of notched tensile and compact tension samples of Al-Li 2090 T8E41 [*8*–

S_
N_

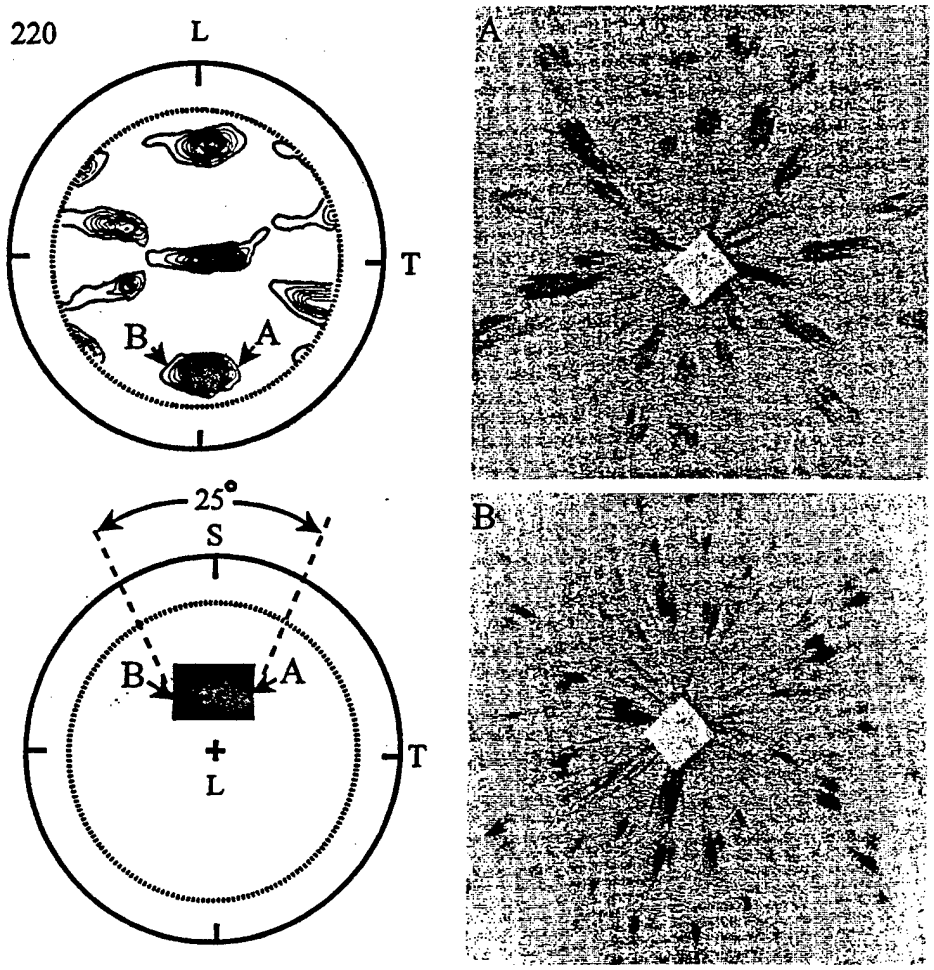

FIG. 8—*Orientation of ⟨110⟩ diffraction ellipses related to the macrotexture of the center of plates of Al-Li 2090 T8E41. The 220 pole figure (after Ref. 14) is shown at the upper left, and the portion of the macrotexture producing the ⟨110⟩ ellipses is represented by the arrows A and B. The range of ellipse orientations is shown in the two diffraction patterns shown to the right. The L-oriented stereographic projection (lower left) relates the experimentally observed ⟨110⟩ zones to the macrotexture: the locus of expected diffracted beam directions are shown for orientations within rectangle in the pole figure.*

13] revealed that the crack faces contacted over a large fraction of their areas at stress intensities substantially higher than K_{cl}. The pattern of contact is very complex, but actual contact on mixed mode surfaces appears to be necessary but not sufficient to produce slowing of crack propagation by the roughness-induced crack closure mechanism. The authors wonder, therefore, whether it might not be more physically reasonable to ascribe the slower crack growth primarily to increased resistance to crack propagation (~~either~~ through increased energy per unit of crack ~~extension~~, ~~the~~ greater crack area due to the ~~and/or per unit area~~ opened) due to forcing the crack through the highly crystallographic path.

Conclusions

A characteristic mesotexture that leads to the formation of asperities and crack closure in fatigue has been shown to be present in Al-Li 2090 T8E41: sets of adjacent grains are so highly aligned that they may be regarded as near-single-crystal volumes. The microbeam Laue patterns show that approximately 45% of the volume of the central portions of plates consist of these near single-crystal regions. While several orientations of the near-single-crystal volumes occur, all are consistent with the macrotexture revealed in pole figures. The large asperities investigated contain grains of only one orientation type; and these produce 111 diffraction streaks along the plate L-T direction in both the perpendicular and parallel diffraction geometries. The results demonstrate that large crack deflections occur when the crack encounters adjacent volumes of near-single-crystal material with different orientations.

The results demonstrate, perhaps for the first time, the importance of mesotexture, the scale of preferred orientation between micro- and macro-texture, in determining materials' response to service conditions such as fatigue. Large levels of fatigue crack closure accompany the extremely low crack propagation rates in L-T orientations of Al-Li 2090 T8E41, and results of a variety of techniques, including high-resolution x-ray computed tomography, demonstrated that the large asperities formed on the fatigue crack surface are key in producing this roughness-induced crack closure. Two factors combine to produce large asperities and extraordinarily crack closure effects: slip and crack propagation is highly planar in Al-Li alloys and the volumes over which planar slip/crack propagation can operate undisturbed are quite large due to the type of mesotexture present. Not only are grain orientations highly correlated, meaning there is strong macrotexture present, but the orientations are also frequently spatially correlated in groups of ~5–20 adjacent grains. It is this feature that, the authors believe, makes Al-Li 2090 T8E41 unique and suggests an avenue for designing improved fatigue crack resistance in future alloys. Finding or producing a similar type of mesotexture in another alloy would be interesting indeed; one hopes the interplay between "forcing" function, mesotexture and crack growth rate would come into clearer focus.

Acknowledgments

We gratefully acknowledge the encouragement of George Yoder, Officer of Naval Research, and support through ONR grants N00014-94-1-0306, N00014-94-1-0726, and N00014-97-1-0557. Experiments were performed at SSRL, which is operated by the Department of Energy, Office of Basic Energy Sciences. We thank Zofia Rek of SSRL for invaluable assistance with the microbeam experiments, R. Brown for help fatiguing samples and S. Spragg and T. Watt for outputting the many diffraction patterns.

References

[1] Venkateswara Rao, K. T., Yu, W., and Ritchie, R. O., *Metallurgical Transactions*, Vol. 19A, 1988, p. 549.

[2] Yoder, G. R., Pao, P. S., Iman, M. A., and Cooley, L. A., in *Proceedings from the 5th International Conference on Aluminum-Lithium Alloys*, T. H. Sanders, Jr. and E. A. Starke, Jr., Eds., *Mat. and Comp. Eng. Publ.*, Birmingham, UK, 1989, p. 1033

[3] Pao, P. S., Cooley, L. A., Iman, M. A., and Yoder, G. R., *Scripta Metallurgica.* Vol. 23, 1989, p. 1455.

[4] Adams, B. L., Wright, S. I., Kunze, K., *Metallurgical Transactions*, Vol. 24A, 1993, p. 819.

[5] Dingley, D. J., *Scanning Electron Microscopy*, Vol. 2, 1984, p. 569.

[6] Ritchie, R. O., in *Fatigue Thresholds,* J. Backland, A. Blom, and C. J. Beevers, Eds., Eng. Advisory Services, Warley, UK, 1981, p. 503.

[7] Ritchie, R. O., *Material Science and Engineering,* Vol. 103, 1988, pp. 15–28.

[8] Breunig, T. M., Stock, S. R., Antolovich, S. D., Kinney, J. H., Massey, W. N., and Nichols, M. C., *ASTM STP 1131,* 1992, p. 749.

[9] Guvenilir, A., Stock, S. R., Barker, M. D., and Betz, R. A., in *Proceeding from the 4th International Conference on Aluminum Alloys,* T. H. Sanders, Jr. and E. A. Starke, Jr., Eds., Georgia Institute of Technology, Atlanta, GA, Vol. II, 1994, p. 4.

[10] Guvenilir, A., Breunig, T. M., Kinney, J. H., and Stock, S. R., *Acta Materialia,* Vol. 45, 1997, p. 197.

[11] Guvenilir, A., *Investigation into Asperity Induced Closure in an Al-Li Alloy Using X-Ray Tomography,* PhD Thesis, Georgia Inst. Of Technology, December 1995.

[12] Guvenilir, A. and Stock S. R., *Fracture and Fatigue of Engineering Materials & Structures,* Vol. 21, 1998, p. 439.

[13] Morano, R., *Effect of R-Ratio on Crack Closure in Al-Li 2090 T8E41, Investigated Non-Destructively with X-ray Microtomography,* MS Thesis, Georgia Institute of Technology, September 1998.

[14] Yoder, G. R., Pao, P. S., Imam, M. A., and Cooley, L. A., *Scripta Metallurgica,* Vol. 22, 1988, p. 1241.

[15] Pao, P. S., Imam, M. A., Cooley, L. A., and Yoder, G. R., *Corrosion,* Vol. 45, 1989, p. 530.

[16] Venkateswara Rao, K. T. and Ritchie, R. O., *Mater. Sci & Technol,* Vol. 5, 1989, p. 882 and p. 896.

[17] Ameniya, Y., Matsushita, T., Nakagawa, A., Satow, Y., Miyahora, J., and Chikawa, J., *Nuclear Instrument Methods,* Vol. A266, 1988, p. 645.

[18] Whiting, B. R., Owen, J. F., and Rubin, B. R., *Nuclear Instrument Methods,* Vol. A266, 1988, p. 688.

[19] Stock, S. R., Rek, Z. U., Chung, Y. H., Huang, P. C., and Ditchek, B. M., *J. Appl. Phys.,* Vol. 73, 1993, p. 1737.

[20] Cullity, B. D., *Elements of X-ray Diffraction,* 2nd Edition, Addison-Wesley Pub., Menlo Park, CA, 1978.

[21] Barlat, F., Miyasota, S. M., Liu, J., and Bren, J. C., in *Proceeding from the 4th International Conference on Aluminum Alloys,* Vol. II, T. H. Sanders, Jr. and E. A. Starke, Jr., Eds., Georgia Institute of Technology, Atlanta, GA, 1994, p. 389.

[22] Sanders, T. H., Jr., Final Report, Naval Air Development Center, Warminster, PA. Contract No. N62269-76-C-0271.

[23] Suresh, S., *Fatigue of Materials,* Cambridge Univ. Press, UK, 1991, p. 194.

S_
N_

Pergamon

Acta mater. Vol. 46, No. 18, pp. 6599–6604, 1998

1359-6454/98 $19.00 + 0.00

PII: S1359-6454(98)00298-5

X-RAY MICROBEAM QUANTIFICATION OF GRAIN SUBDIVISION ACCOMPANYING LARGE DEFORMATIONS OF COPPER

A. GUVENILIR†[1], G. C. BUTLER[2], J. D. HAASE[1], D. L. MCDOWELL[1,2] and S. R. STOCK[1]‡

[1]School of Materials Science and Engineering, Mechanical Properties Research Laboratory, Georgia Institute of Technology, Atlanta, GA 30332-0245, U.S.A. and [2]George W. Woodruff School of Mechanical Engineering, Mechanical Properties Research Laboratory, Georgia Institute of Technology, Atlanta, GA 30332-0245, U.S.A.

(Received 10 March 1998; received in revised form 8 July 1998; accepted 5 August 1998)

Abstract—This work reports the application of X-ray microbeam diffraction to quantifying grain subdivision processes in copper. Polychromatic synchrotron X-radiation was used to study samples in the as-received (low deformation) and 100% torsion strained material. The large range of domain disorientations (within individual grains) observed in the highly strained material agrees with results on other f.c.c. materials obtained by electron beam methods; it is not surprising, therefore, that models of texture development which do not include this effect predict too rapid sharpening of preferred orientation compared to experimental pole figures. © *1998 Acta Metallurgica Inc. Published by Elsevier Science Ltd. All rights reserved.*

1. INTRODUCTION

On the scale of the individual grain, the crystalline lattice dictates that material properties are highly directional while the anisotropy of macroscopic average properties depends on the randomness of grain orientations. The pattern of preferred orientation is termed texture, and several scales of texture have been identified: macro-, meso- and microtexture and subgrain domains. Macrotexture refers to the average texture of a sample, microtexture the orientation of individual grains, and mesotexture the orientation of ensembles of adjacent grains [1], i.e. a local average as opposed to a sample average texture. Despite experimental estimates that subgrain structures contribute levels of anisotropy comparable to grain reorientation up to moderate strains [2], relatively little attention has focused on this source of orientation anisotropy accompanying large deformations.

The Taylor model [3,4] applied to texture development [5–7] represents the qualitative aspects of texture distribution reasonably well, but experiment shows a less sharp, more slowly developing texture than predicted [8,9]. Treatment of grains as discrete entities largely ignores the development of substructure and the accompanying rotations between domains observed within grains. For example, disorientations $>10°$ between adjacent ($\sim 1\ \mu m$) domains are common in f.c.c. materials after equivalent von Mises strains $\epsilon_{vM} > 1$ [10]. It is difficult to see how models could match experiment without incorporating this effect.

Quantification of preferred orientation or macrotexture began with Wever [11] and is a standard component of undergraduate materials curricula, e.g. textbooks on X-ray diffraction [12,13]. Recent work emphasizes orientation imaging microscopy or OIM [14,15] for microtexture measurements used to construct macrotexture pole figures [16] or for quantification of disorientations between adjacent grains [17] or transmission electron microscopy (TEM) for quantification of subgrain domain disorientations [10,18]. Electron beam techniques require significant sample preparation: OIM requires largely strain-free surfaces or the channeling patterns degrade to the point where they cannot be analyzed, and TEM samples must be extremely thin foils. X-ray microbeam diffraction is very attractive, however, for three-dimensional microtexture quantification and for microtexture evolution studies.

The availability of dedicated synchrotron radiation facilities renewed interest in X-ray microbeam diffraction [19–21]. Recently transmission Laue patterns of 2–3 mm thick samples of Al–Li 2090 T8E41 revealed mesotexture consisting of groups of adjacent grains which are so closely aligned that

†Presently at: Motorola, M/D K-10, Yield Enhancement Technology Transfer, 3501 Ed Bluestein Blvd, Austin, TX, U.S.A.

‡To whom all correspondence should be addressed. Tel.: +1 (404) 894-6882; Fax: +1 (404) 894-9140; E-mail: stuart.stock@mse.gatech.edu.

this volume of material can be termed near-single-crystalline [1]. Mapping with 1 μm diameter or smaller X-ray microbeams will soon be routine [22, 23].

This paper reports the first application of microbeam X-ray diffraction to quantification of grain subdivision, i.e. measuring disorientations between adjacent domains. Comparison of Laue patterns from as-received and 100% torsion deformed Cu samples forms the basis of the work.

2. EXPERIMENTS

The samples were OFHC (oxygen-free high conductivity) Cu with an initial grain size of approximately 60 μm [24]. One sample was cut from the as-received material, and the second was cut from a thin-walled tubular specimen strained in free-end torsion to 100%. The thin-walled torsion specimen design, adapted from that of Lindholm *et al.* [25], limits deformation to the gage section, even at large strains, and maintains a high degree of shear strain uniformity in this volume. The free-end torsion test was conducted at room temperature at an effective strain rate of 4×10^{-4} s^{-1} using a closed-loop servo-hydraulic, axial-torsional test machine. Pole figures from 111, 200 and 220 reflections were measured from these two samples as well as others with different loading path complexities, and these results are reported elsewhere [26]. The observed macrotextures of the samples, in particular the 100% torsion sample, were consistent with those reported in the literature.

Planar sections of both samples were cut with a slow speed diamond wheel. The sample from the walls of the 100% torsion sample was cut parallel to the shear plane (i.e. normal to the specimen axis). Both samples were ground by hand from 1 mm thick sections into wedges, and both sides were metallographically polished on SiC paper and were etched to remove polishing damage. The portion of the samples examined with the X-ray microbeam was about 100 μm and no more than 200 μm thick.

All diffraction data were collected with polychromatic bending magnet radiation at the SSRL beamline 2–2 (3.0 GeV, beam currents between 100 and 50 mA). Transmission Laue patterns were recorded using a 10 μm diameter pinhole collimator and Fuji image storage plates, and exposures were on the order of 4×10^4 mA.s. The collimator was placed 55 cm from the sample in order to minimize the effect of scatter from the edges of the pinhole, and the ~20 arcseconds of vertical divergence of the beam was enough to broaden the beam from the 10 μm diameter collimator to 80 μm vertically at the sample position [27]. Both the image storage plate and the wedge-shaped samples were normal to the incident beam, and a Fuji BAS-2500 Imaging Plate Scanner was used to read the 20×40 cm^2 plates with 50 μm pixel resolution and 256 levels of contrast.

Beams diffracted from the specimen passed through 3 mm of Al on the front of the holder for the image plates. A diamond-shaped, Pb beam stop was attached to the front of the plate holder, its shadow is prominent in the diffraction patterns and its thickness allowed the incident beam to produce a weak image on the plate. For some of the diffraction patterns, Pd, Zr or Mo absorption edge filters were used to identify hkl for the different diffraction streaks [28] and to insure that 111 streaks were compared for the two samples.

Microtexture was mapped by translating each sample perpendicular to the beam by 10 μm steps and recording the resulting transmission Laue pattern. While the column of irradiated material was wider than the starting grain size, comparison of diffraction patterns after 10 μm translations allowed the grain subdivisions to be distinguished.

3. RESULTS AND DISCUSSION

Figure 1 compares typical diffraction patterns from the as-received (nominally undeformed) sample (a) and the sample tested to 100% torsion (b). The numbers label streaks or groups of streaks while the white squares to either side of the streaks or groups of streaks mark the position where the change of contrast from the Pd K absorption edge (0.509 Å) would have been observed were the filter in the beam. The difference is striking between the patterns of the as-received material and the 100% torsion sample. Narrow, discrete radial streaks comprise the pattern of the as-received sample while the torsion sample's pattern consists of many radial streaks grouped in envelopes of differing azimuthal orientations. The presence of the expected small amount of deformation in the as-received samples alters the spots of the Laue pattern into streaks with lengths similar to those of the 100% torsion sample. The azimuthal widths of the streaks or groups of streaks, however, does reflect the difference in deformation over the scale of the particular image.

Figure 2(a) shows diffracted intensity as a function of azimuthal angle for the diffraction pattern of the as-received sample [shown in Fig. 1(a)], and Fig. 2(b) shows that for the 100% torsion sample [shown in Fig. 1(b)]. The intensity was measured along the locus of points where 111 diffracts the wavelength of the Pd K-edge. The results shown in Fig. 2 change very little if the radius of the measuring circle is altered. The azimuthal angle is zero at the twelve o'clock position and increases clockwise. The four largest peaks in the plot of Fig. 2(a), from left to right, are streaks 4, 5, 1 and 2 in Fig. 1(a). In Fig. 2(b) streak 8 lies between ~90° and ~120°, streak 1 lies between ~135° and 170° and streak 6 lies between ~190° and ~230°. Within streak 8

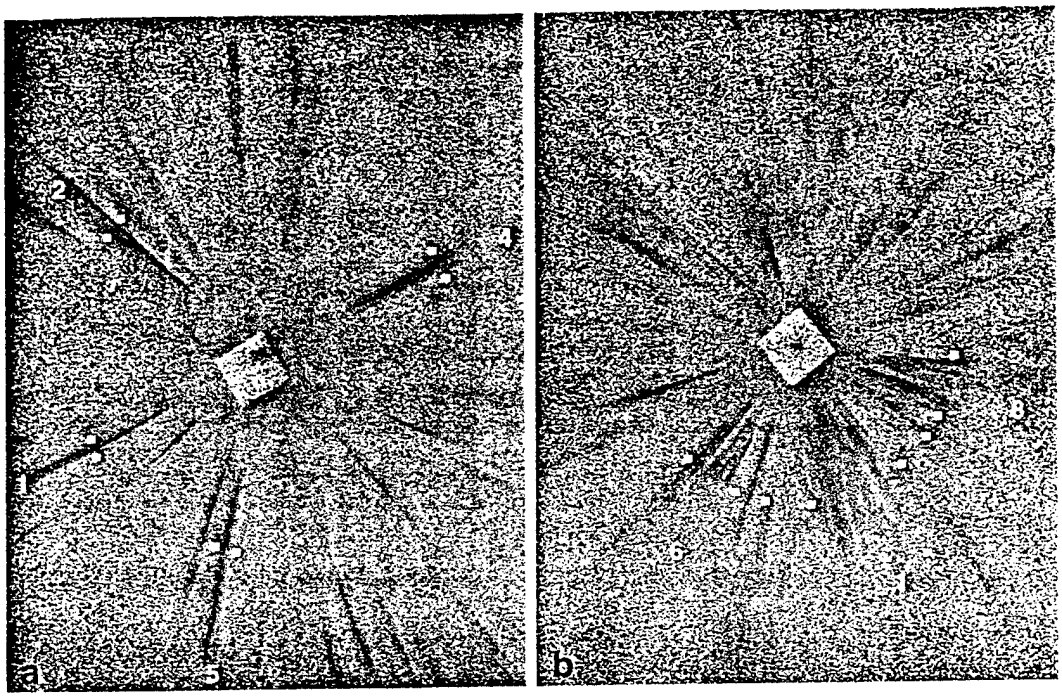

Fig. 1. Comparison of Laue patterns from (a) undeformed and (b) 100% torsion samples. The numbers label streaks or groups of streaks while the white squares appear at either side of streaks and indicate the positions where the change of contrast from the Pd K-absorption edge were observed for 111 diffraction. The circular loci of the edge wavelength have different radii because different film-to-sample separations were used.

there are three substreaks a–c [from left to right in Fig. 2(b) or in a clockwise sense in Fig. 1(b)], within streak 1 there are four substreaks and within streak 6 there are also four substreaks.

Table 1 summarizes the azimuthal angular widths of the streaks in Figs 1 and 2. In the as-received state, the full width (FW) of the streaks (measured at background intensity) ranged between ~4.5° and

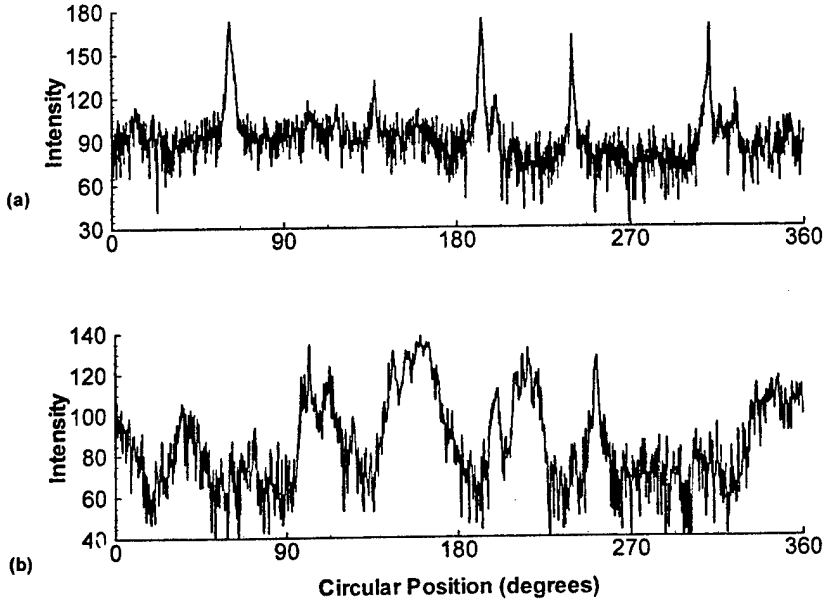

Fig. 2. Plot of diffracted intensity as a function of azimuthal angle for the Laue patterns in Fig. 1; the measurement was made at the position for 111 diffraction of the wavelength of the Pd K edge. Plots (a) and (b) are from the undeformed and 100% torsion samples, respectively. The azimuthal angular measurement begins at the twelve o'clock position in Fig. 1 and proceeds clockwise.

Table 1. Azimuthal peak widths for the as-received and 100% torsion samples, where FW is the full width, FWHM is the full width at half-maximum diffracted intensity and the letters denote the substreaks (as encountered during clockwise rotation from vertical in Fig. 2) between the boundaries of which the angular separation is measured in the 100% torsion sample

Sample	Streak	FW (°)	FWHM (°)				
As-received	4	9.1	4.6				
	5	7.3	3.5				
	1	4.6	2.1				
	2	7.6	2.4	Substreak separations (°)			
				a–b	b–c	c–d	d–e
100% Torsion	8	43.7	29.9	7.6	6.8	4.0	
	1	31.2	27.2	9.5	3.5	2.7	4.3
	6	31.7	28.5	1.8	2.5	10.7	11.8

~9°, and the full-width at half-maximum diffracted intensity (FWHM) ranged between 2.0° and 4.5°. After 100% torsion, the streaks' FW ranged between ~31° and ~44° while FWHM values were between 27° and 29°; no features of comparable azimuthal width were ever observed in the as-received sample. Substreak separations in the 100% torsion sample ranged between 2° and 12° and indicated inhomogeneous deformation broke the grain into discrete, significantly-disoriented domains.

Figure 3, of the 100% torsion sample, shows a line of six Laue patterns recorded 10 μm apart. In Fig. 3(c), the pattern is the same as that shown in Fig. 1(b), and the white circle indicates where 111 diffracts the Pd K-edge wavelength. Streak 6 is not present in Fig. 3(a), becomes prominent in Figs 3(b)–(e) and disappears rather abruptly between Figs 3(e) and (f). Streak 8 follows a similar pattern. Portions of streak 1 are already present in Fig. 3(a) and disappear over the next 50 μm while

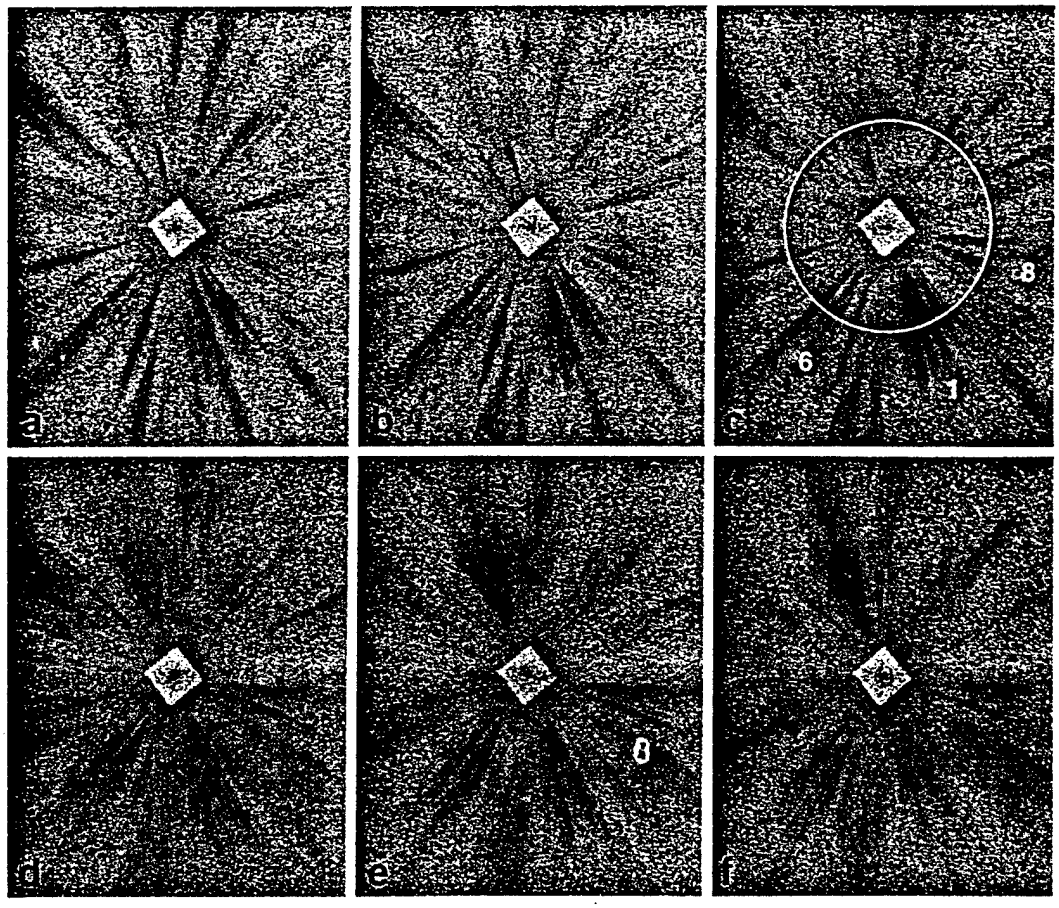

Fig. 3. Six Laue patterns recorded at adjacent positions separated by 10 μm translation steps.

new substreaks appear in Fig. 3(c) and disappear by the position where Fig. 3(f) was recorded. With a beam diameter slightly less than 80 μm, the patterns in Fig. 3 overlapped significantly, and the results are consistent with a 10 μm or smaller domain size.

The small number of 111 streaks or groups of streaks observed in any one Laue pattern is expected from the initial grain size, the beam diameter and the small sample thickness. The change from sharp, individual streaks to envelopes of substreaks after 100% torsion corresponds to formation of individual domains within each original 60 μm diameter grain: otherwise, even if sharp macrotexture were present, the streaks would appear and disappear more randomly than in Fig. 3. The fact that the groups of streaks persist over translations on the order of 50–100 μm, i.e. the original grain size, also indicates that the domains producing each streak of the group originated from a single grain. While the microbeam diameter used here does not allow detailed comment on the disorientation between adjacent domains after 100% torsion, the substreak separations are often $>5°$, indicating that adjacent domains must be disoriented more than this, in agreement with recent TEM results on other heavily deformed f.c.c. materials [10, 18].

The present results have important implications for modeling macrotexture accompanying large deformations (and complex loading histories, e.g. compression followed by torsion) in Cu and other f.c.c. materials. It appears that grain subdivision processes must be incorporated if macrotexture sharpening rates are to be correctly predicted. One expects that the significant interest engendered by the new generation of storage rings will soon lead to microtexture studies with microbeam X-ray diffraction of 10 μm or smaller diameter columns of irradiated material. In fact recent improvements in shielding have allowed the collimator to be moved within 2–3 cm of the Cu sample before scatter seriously affects the quality of the Laue patterns; the column of material irradiated was between 15 and 20 μm wide. Data for various heavily deformed Cu samples has been collected and is currently being analyzed. The speed with which large volumes of material may be interrogated make X-ray microbeam orientation mapping with polychromatic synchrotron radiation very attractive indeed.

4. CONCLUSIONS

The results presented demonstrate that microbeam diffraction using polychromatic synchrotron X-radiation can be used to quantify grain subdivision accompanying high levels of deformation in copper, even when the beam diameter is somewhat larger than the grain size in the undeformed material. The measured disorientations between domains from single grains are consistent with those measured by others for other f.c.c. materials, and the results suggest that the reason that Taylor models predict macrotextures much sharper than experiment is they do not yet account for the spread of orientations produced by the grain subdivision processes.

Acknowledgements—We thank Mr S. Graham Jr of the MPRL for conducting the 100% torsion experiment and Dr Z. U. Rek of SSRL for her assistance. The data were recorded at SSRL which is supported by the Department of Energy. We are also grateful for support from the Office of Naval Research (through grants N00014-94-1-0306 and -0726) and from the Army Research Office (through grants DAAH0493G00138 and DAAH049510177).

REFERENCES

1. J. D. Haase, A. Guvenilir, J. R. Witt and S. R. Stock, *Acta mater.*, 1998, **46**, 4791.
2. Hansen, N. and Jensen, D. J.. *Acta metall. mater.*, 1992, **40**, 3265.
3. Taylor, G. I., *J. Inst. Metals*, 1938, **62**, 307.
4. G. I. Taylor, in *Steven Timoshenko 60th Anniv. Vol.*, ed. J. M. Lessels, 1938, p. 218.
5. Asaro, R. J. and Needleman, A., *Acta metall.*, 1985, **33**, 923.
6. Mathur, K. K. and Dawson, P. R., *Int. J. Plasticity*, 1989, **5**. 67.
7. S. R. Kalidindi and L. Anand, in *Adv. in Finite Deformation Prob.in Mater. Processing and Structures*, AMD **125**, ed. N. Chandra and J.N. Reedy. ASME, 1991, p. 3.
8. Hansen, N. and Kuhlman-Wilsdorf, D., *Mater. Sci. Eng.*, 1986, **81**, 141–161.
9. M. G. Stout, J. S. Kallend, U. F. Kocks, M. A. Przystupa and A. D. Rollett, in *Proc. 8th Conf. on Textures of Mater. (ICOTOM 8)*, ed. J. S. Kallend and G. Gottstein. TMS, 1988, p. 479.
10. Hughes, D. A. and Hansen, N., *Acta mater.*, 1997, **45**, 3871.
11. Wever, F., *Z. Phys.*, 1924, **28**, 69.
12. B. D. Cullity, *Elements of X-ray Diffraction*, 2nd edn. Addison–Wesley, Reading, MA, 1978.
13. C. S. Barrett and T. B. Massalski, *Structure of Metals*, 3rd edn. Pergamon Press, Oxford, 1986.
14. Dingley, D. J., *Scanning Electron Microscopy*, 1984, **2**, 569.
15. Randall, V., *Microtexture Determination and its Applications*. Institute of Metals, 1992.
16. Adams, B. L., Wright, S. I. and Kunze, K., *Metal. Trans.*, 1993, **24A**, 819.
17. Matsumoto, K., Shibayanagi, T. and Umakoshi, Y., *Acta mater.*, 1997, **45**, 439.
18. Hughes, D. A., Liu, Q., Chrzan, D. C. and Hansen, N., *Acta mater.*, 1997, **45**, 105.
19. Stock, S., Ice, G. E., Habenschuss, A. and Sparks Jr, C. J., National Synchrotron Light Source Annual Report 1986, BNL 52045, p. 354.
20. Rebonato, R., Ice, G. E., Habenschuss, A. and Bilello, J. C., *Phil. Mag. A*, 1989, **60**, 571.
21. Ice, G.E., *summarizing [19 and 20], Nucl. Instrum. Meth., 1987*, **B24-25**(1), 397.
22. Wang, P. C., Cargill, G. S. III and Noyan, I. C., *Water Res. Soc. Proc.*, 1995, **375**, 247.

23. Poulsen, H. F., Garbe, S., Lorentzen, T., Juul Jensen, D., Poulsen, F. W., Andersen, N. H., Frello, T., Feidenhansl, R. and Graafsma, H., *J. Synchrotron Radiat.*, 1997, **4**, 147.
24. Graham Jr, S. M.S. thesis, Georgia Institute of Technology, 1995.
25. Lindholm, U. S., Nagy, A., Johnson, G. R. and Hoegfeldt, J. M., *ASME J. Engng Mater. Technol.*, 1980, **102**, 376.
26. Butler, G. C., Graham, S., McDowell, D. L., Stock, S. R. and Ferney, V. C., *ASME J. Engng Mater. Technol.* 1998, **120**, 197.
27. Stock, S. R., Langøy, M. A. and Morano, R. unpublished data, December 1997.
28. Stock, S. R., Rek, Z. U., Chung, Y. H., Huang, P. C. and Ditchek, B. M., *J. appl. Phys.*, 1993, **73**, 1737.